Explicit isogeometric collocation for the dynamics of three-dimensional beams undergoing finite motions

Explicit isogeometric collocation for the dynamics of three-dimensional beams undergoing finite motions

Enzo Marino[a,c,*], Josef Kiendl[b], Laura De Lorenzis[c]

[a] *Department of Civil and Environmental Engineering – University of Florence, Via di S. Marta 3, 50139 Firenze, Italy.*
[b] *Department of Marine Technology – Norwegian University of Science and Technology, NO-7491 Trondheim, Norway.*
[c] *Institute of Applied Mechanics – TU Braunschweig, Pockelsstraße 3, 38106 Braunschweig, Germany.*

Abstract

We initiate the study of three-dimensional shear-deformable geometrically exact beam dynamics through explicit isogeometric collocation methods. The formulation we propose is based on a natural combination of the chosen finite rotations representation with an explicit, geometrically consistent Lie group time integrator. We focus on extending the integration scheme, originally proposed for rigid body dynamics, to our nonlinear initial-boundary value problem, where special attention is required by Neumann boundary conditions. The overall formulation is simple and only relies on a geometrically consistent procedure to compute the internal forces once control angular and linear accelerations of the beam cross sections are obtained from the previous time step. The capabilities of the method are shown through numerical applications involving very large displacements and rotations and different boundary conditions.

Keywords: Isogeometric collocation, Explicit dynamics, Geometrically nonlinear Timoshenko beams, Finite rotations

1. Introduction

The study of isogeometric collocation (IGA-C) methods has been recently initiated in [1, 2] motivated by the idea of taking advantage from the higher-order and higher-smoothness NURBS basis functions used in isogeometric analysis (IGA) and the low computational cost

*Corresponding author
Email address: enzo.marino@unifi.it (Enzo Marino)

of collocation. IGA was introduced in 2005 by Hughes et al. [3] with the primary goal of representing the exact geometry regardless of the mesh refinement level and simplifying the expensive operations of mesh generation and refinement required by traditional Finite Element Analysis (FEA). Additionally, thanks to the higher-order basis functions with tailorable smoothness, IGA has proven to achieve increased accuracy and robustness on a per degree-of-freedom basis compared with standard FEA [4–7]. However, in IGA the problem of finding optimal quadrature rules able to fully exploit the high inter-element continuity is still open, although recently substantial progress was achieved [8–10]. IGA-C naturally circumvents this issue since it is based on the discretization of the strong form of the governing equations where the presence of higher-order derivatives is not an issue due to the smoothness of the basis functions. In addition to the complete elimination of numerical quadrature, IGA-C requires only one evaluation (collocation) point per degree of freedom, regardless of the approximation degree. These attributes make the method much faster than standard Galerkin-based IGA and FEA [11]. After the initial focus on elasticity [1, 2] and other linear problems [11], further applications of IGA-C were proposed for phase-field modeling [12], contact problems [13, 14] and hyperelasticity [14]. Also, new connections between Galerkin and collocation methods were found in [15]. IGA-C has already been successfully applied to one- and two-dimensional structural problems. Locking-free formulations for Timoshenko beams were proposed in [16–19]. An IGA-C approach for Bernoulli-Euler beams and Kirchhoff plates was proposed in [20]. Reissner-Mindlin plate and shell problems were addressed in [21] and [22], respectively. Kirchhoff-Love plate and shell problems were studied in [23]. In [24, 25] IGA-C was extended to geometrically exact shear-deformable beams, including frictionless contact in [26]. Locking-free formulations for geometrically nonlinear spatial beams were proposed in [25, 27] and, very recently, an implicit dynamic IGA-C formulation was proposed in [28].

A field where the IGA-C attributes have a significant impact is explicit dynamics. Here the idea is to keep the computational advantages of one-point quadrature methods and, at the same time, achieve high-order accuracy avoiding stabilization techniques. An explicit IGA-C method was introduced by Auricchio et al. [2], where a higher-order space-accurate predictor-multicorrector algorithm was proposed and applied to one and two-dimensional

linear elastic cases. Very recently, Evans et al. [29] developed explicit higher-order space- and time-accurate IGA-C methods for linear elastodynamics. They introduced a semi-discrete reinterpretation of the predictor-multicorrector approach and showed that for pure Dirichlet problems it is possible to obtain second-, fourth-, and fifth-order accuracy in space with one, two, and three corrector passes, respectively. For pure Neumann and mixed Dirichlet-Neumann problems, it is possible to achieve second- and third-order accuracy in space with one and two corrector passes, respectively. Additionally, higher-order accuracy in time is achieved in [29] using the fully discrete predictor-multicorrector algorithms within explicit Runge-Kutta methods.

Following the route opened in [24, 27], in this work we extend the development of the IGA-C method to the explicit dynamics of three-dimensional beams undergoing finite motions. The kinematic beam model we consider is commonly referred to as geometrically exact, namely able to describe three-dimensional displacements and rotations without any restriction in magnitude and direction and the associated strain measures are derived without introducing any approximation. We start exploring this field having in mind that the ultimate goal is the development of robust, efficient and high-order space (and possibly time) accurate methods suitable for transient analysis involving finite motions with a potential for all the structural elements, such as plates and shells, which share similar kinematic features to the present beam model. As pointed out in [29], apparently this objective cannot be achieved without removing one of the most critical simplifications in explicit dynamics: the lumped mass matrix. The most promising countermeasure to avoid equation-solving costs arising from a consistent mass matrix seems to be the predictor-multicorrector algorithm [2, 29]. Unfortunately, unlike in linear and traditional nonlinear structural dynamics, in the case addressed in this work the configuration space involves the rotation (Lie) group SO(3) where standard time integration schemes, including predictor-multicorrector methods, cannot be straightforwardly used. Thus, in this work we employ consistent mass and inertia matrices and focus mainly on the development of a geometrically SO(3)-consistent explicit time integration scheme. This first step prepares the ground for a following development specifically aimed at finding methods to avoid equation-solving suitable for SO(3).

Over the last thirty years, starting in 1988 with the fundamental works by Simo & Vu-

Quoc [30] and Cardona & Geradin [31], a large number of formulations, mainly based on standard FEA, have been proposed for the dynamics of geometrically exact spatial beams and pro and cons of different time integration schemes have been discussed in a number of papers [28, 32–45]. Reviews of the topic can be found in [46, 47]. In the present work, finite rotations are represented by elements of SO(3) and incremental rotations are parameterized by means of spatial rotation vectors. As in [30, 48, 49] configuration updates are made directly by exponentiating and superimposing the incremental rotation to the current rotation. The update operation crucially relies on the exact expression of the exponential map, which maps infinitesimal rotations belonging to so(3) onto elements of SO(3). The choice of this kinematic model has a number of advantages, especially in an explicit dynamic context where incremental rotations are very small due to the time step size. Firstly, the method is geometrically consistent in that updated rotations naturally remain in SO(3) and no additional equations need to be collocated as in the case of quaternion-based models to guarantee the orthogonality of the rotation operator. Secondly, there is no need to introduce the linear transformation commonly used to project incremental rotations belonging to different tangent spaces to SO(3). As a consequence, issues related to its exact differentiation [31, 50, 51] are removed and a very simple formulation is obtained which only (but crucially) relies on the consistent updating procedure. Thirdly, the kinematic model is naturally singularity-free due to the small time step size. Finally, and even more importantly, the kinematic model we employ can be easily combined with one of the best-performing explicit Newmark time integration method for SO(3). The algorithm, which was proposed by Krysl & Endres in [52] for the rotational dynamics of rigid bodies, was proven to attain, or even improve, the performances of the two most popular existing explicit methods for rigid body dynamics, see [53, 54]. The algorithm is obtained from the standard Newmark scheme by setting $\gamma = 1/2$ and $\beta = 0$, so that it becomes a second-order accurate explicit central difference method. One of the key attribute, which also motivated the choice of this algorithm, is that with this specific choice of γ, the update formula for the angular velocity takes the same simple form of the translational velocity, avoiding again the use of linear projections between tangent spaces. We note also that the choice of this explicit method bypasses the arguments about the geometric consistency of the SO(3) Newmark scheme raised in [35]. The extension of

the time integrator to the flexible shear-deformable beam is straightforward, with the remarkable advantage of not requiring the linearization of the governing equations. Update of the right-hand sides of the governing equations is performed through a simple geometrically consistent procedure once control values of angular and linear accelerations, which are our primary variables, are computed from the previous time step. As opposed to the equations collocated in the interior points, where the pointwise kinematic analogy with the rigid body dynamics is directly exploited, special attention is paid to Neumann boundary conditions which need to be linearized.

The outline of the paper is as follows: in Section 2 we briefly review the three-dimensional shear-deformable beam theory highlighting the key geometric aspects which will play a crucial role in the development of the formulation. In Section 3 we present the time and space discretizations of the governing equations as well as the boundary and initial conditions; also, we discuss the consistent time update procedure. In Section 4 we present the solution method and in Section 5 we apply the proposed formulation to solve problems involving very large displacements and rotations and with different boundary conditions. Finally, in Section 6, we summarize and draw the main conclusions of our work.

2. A brief review of the shear-deformable beam theory

In this section we briefly review the shear-deformable beam theory. We start with the geometric structure of the beam kinematics, then we present the balance equations and finally we introduce the constitutive equations.

2.1. Kinematics

The motion $\boldsymbol{\varphi} : \boldsymbol{T} \times \mathcal{B} \to \boldsymbol{E}$ of a shear-deformable beam $\mathcal{B}$ is expressed as follows

$$\boldsymbol{\varphi}(t, \boldsymbol{p}) = \boldsymbol{c}(t, \boldsymbol{q}) + \mathbf{R}(t, \boldsymbol{q})(\boldsymbol{p} - \boldsymbol{q}) \quad \text{for each} \quad t \in \boldsymbol{T}\,, \boldsymbol{p} \in \mathcal{B}\,, \tag{1}$$

where $\boldsymbol{E}$ is the Euclidean space, $\boldsymbol{T}$ is the time domain and $\boldsymbol{q}$ is the centroid of the beam cross section containing point $\boldsymbol{p}$ (see Figure 1). The set of the centroids of all cross sections is a one-dimensional space $\mathcal{S} \subset \mathcal{B}$ that we call centroid line. The fundamental kinematic assumption expressed by Eq. (1) permits describing the motion of any material point $\boldsymbol{p}$ of

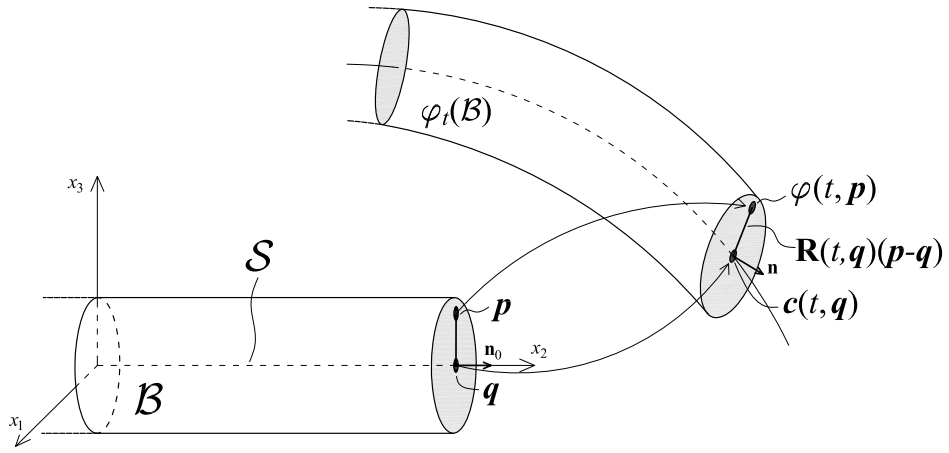

Figure 1: Sketch of the motion of a three-dimensional shear deformable beam.

the beam through the motion $\boldsymbol{c}$ of the cross section centroid and the rigid rotation $\mathbf{R}$ of the beam cross section. Therefore, a configuration of the beam is determined by the pair $(\boldsymbol{c}, \mathbf{R})$, where we remark that $\boldsymbol{c}$ is a map onto $\boldsymbol{E}$ and $\mathbf{R}$ is a map onto the Special Orthogonal group SO(3). This directly leads to the definition of the configuration manifold as follows

$$\mathcal{C} = \{(\boldsymbol{c}, \mathbf{R}) \,|\, \boldsymbol{c} : \boldsymbol{T} \times \mathcal{S} \to \boldsymbol{E}\,, \mathbf{R} : \boldsymbol{T} \times \mathcal{S} \to \mathrm{SO}(3)\}\ . \tag{2}$$

The tangent space to the configuration manifold at point $(\boldsymbol{c}, \mathbf{R}) \in \mathcal{C}$ is given by $T_{(\boldsymbol{c},\mathbf{R})}\mathcal{C} = T_{\boldsymbol{c}}\boldsymbol{E} \times T_{\mathbf{R}}\,\mathrm{SO}(3)$, where the tangent space $T_{\boldsymbol{c}}\boldsymbol{E}$ is simply made of vectors $\boldsymbol{\eta}$ applied in $\boldsymbol{c}$, whereas the (spatial) tangent space to SO(3) at $\mathbf{R}$ is given by $T_{\mathbf{R}}\,\mathrm{SO}(3) = \left\{\tilde{\boldsymbol{\vartheta}}\mathbf{R} \,|\, \tilde{\boldsymbol{\vartheta}} \in \mathrm{so}(3)\,, \mathbf{R} \in \mathrm{SO}(3)\right\}$ [30, 38]. From the physical point of view, $\boldsymbol{\eta}$ represents an incremental displacement superimposed to the current configuration of the centroid line $\boldsymbol{c}$; whereas $\widetilde{\boldsymbol{\vartheta}}$, such that $\widetilde{\boldsymbol{\vartheta}}\mathbf{R} \in T_{\mathbf{R}}\,\mathrm{SO}(3)$, represents an incremental rotation superimposed to the current rotation field $\mathbf{R}$[1]. Note that we have chosen the spatial formulation (left translation) for the construction of the tangent space. An equivalent approach, leading to the material tangent space, can be used by employing a right translation of the current rotation $\mathbf{R}$ [31, 35, 37, 38]. We will come back to this later in Section 3 since tangent spaces

[1]The symbol $\sim$ is used to denote elements of so(3), which is the set of 3×3 skew-symmetric matrices. Moreover, given any skew-symmetric matrix $\widetilde{\boldsymbol{a}} \in \mathrm{so}(3)$, $\boldsymbol{a} = \mathrm{axial}(\widetilde{\boldsymbol{a}})$ indicates the axial vector of $\widetilde{\boldsymbol{a}}$ such that $\widetilde{\boldsymbol{a}}\boldsymbol{h} = \boldsymbol{a} \times \boldsymbol{h}$, for any $\boldsymbol{h} \in \mathbb{R}^3$. so(3) represents the Lie algebra of SO(3), namely the tangent space to SO(3) at the identity [55].

play a crucial role in setting geometrically consistent time-stepping schemes. For a complete exposition of the geometric structure underlying the beam kinematics we refer to [48].

2.2. Balance equations in local form

The strong form of the balance equations [56] is given as follows

$$\mu \boldsymbol{a} = \boldsymbol{n}_{,s} + \bar{\boldsymbol{n}} \qquad \text{with} \quad s \in (0, L) \quad \text{and} \quad t \in (0, T]\,, \tag{3}$$

$$\boldsymbol{j}\boldsymbol{\alpha} + \widetilde{\boldsymbol{\omega}}\boldsymbol{j}\boldsymbol{\omega} = \boldsymbol{m}_{,s} + \boldsymbol{c}_{,s} \times \boldsymbol{n} + \bar{\boldsymbol{m}} \qquad \text{with} \quad s \in (0, L) \quad \text{and} \quad t \in (0, T]\,. \tag{4}$$

Boundary and initial conditions in the spatial form are given as follows

$$\boldsymbol{\eta} = \bar{\boldsymbol{\eta}}_c \quad \text{or} \quad \boldsymbol{n} = \bar{\boldsymbol{n}}_c \quad \text{with} \quad s = \{0, L\}\,, t \in [0, T]\,, \tag{5}$$

$$\boldsymbol{\vartheta} = \bar{\boldsymbol{\vartheta}}_c \quad \text{or} \quad \boldsymbol{m} = \bar{\boldsymbol{m}}_c \quad \text{with} \quad s = \{0, L\}\,, t \in [0, T]\,, \tag{6}$$

$$\boldsymbol{v} = \boldsymbol{v}_0 \quad \text{with} \quad s \in (0, L) \quad \text{and} \quad t = 0\,, \tag{7}$$

$$\boldsymbol{\omega} = \boldsymbol{\omega}_0 \quad \text{with} \quad s \in (0, L) \quad \text{and} \quad t = 0\,. \tag{8}$$

In Eqs. (3)-(8), $\boldsymbol{n}$ and $\boldsymbol{m}$ are the internal forces and moments, respectively; $\bar{\boldsymbol{n}}$ and $\bar{\boldsymbol{m}}$ are the distributed external forces and moments per unit length; $\bar{\boldsymbol{n}}_c$ and $\bar{\boldsymbol{m}}_c$ are the external concentrated forces and couples applied to any of the beam ends in the current configuration; $\bar{\boldsymbol{\eta}}_c$ and $\bar{\boldsymbol{\vartheta}}_c$ are the prescribed displacement and rotation vectors at any of the beam ends in the current configuration; μ is the mass per unit length of the beam; $\boldsymbol{j}$ is the spatial inertia tensor, which is related to the material (time-independent) inertia tensor $\boldsymbol{J}$ by $\boldsymbol{j} = \mathbf{R}\boldsymbol{J}\mathbf{R}^{\mathsf{T}}$; $\widetilde{\boldsymbol{\omega}} = \dot{\mathbf{R}}\mathbf{R}^{\mathsf{T}}$ is the spatial skew-symmetric angular velocity tensor and $\boldsymbol{\omega} = \text{axial}(\widetilde{\boldsymbol{\omega}})$ its axial vector; $\boldsymbol{\alpha} = \dot{\boldsymbol{\omega}}$ is the spatial angular acceleration vector; $\boldsymbol{v} = \dot{\boldsymbol{c}}$ and $\boldsymbol{a} = \dot{\boldsymbol{v}}$ are the spatial velocity and acceleration vectors of the cross section centroid; $s \mapsto \boldsymbol{c}_t(s)$ defines the position of the centroid of the beam cross section in the three-dimensional Euclidean space $\boldsymbol{E}$ at time $t \in \boldsymbol{T}$.

With $()_{,s}$ we indicate the partial derivative with respect to the curvilinear coordinate $s : \mathcal{S} \to [0, L] \subset \mathbb{R}$, where L is the length of the beam centroid line in the initial configuration, while with $\dot{()}$ we indicate the partial derivative with respect to time. In the following, especially in the case of basis functions, first and second-order derivatives with respect to s will also be indicated by $()'$ and $()''$, respectively.

The internal stress resultants and deformation measures in the material form are given by

$$\boldsymbol{N} = \mathbf{R}^{\mathsf{T}}\boldsymbol{n} \quad \text{and} \quad \boldsymbol{M} = \mathbf{R}^{\mathsf{T}}\boldsymbol{m}\,, \tag{9}$$

$$\boldsymbol{\Gamma}_N = \mathbf{R}^{\mathsf{T}}\boldsymbol{c}_{,s} - \mathbf{R}_0^{\mathsf{T}}\mathbf{n}_0 \quad \text{and} \quad \boldsymbol{K}_M = \text{axial}(\widetilde{\boldsymbol{K}} - \widetilde{\boldsymbol{K}}_0) = \boldsymbol{K} - \boldsymbol{K}_0\,, \tag{10}$$

where $\boldsymbol{N}$ and $\boldsymbol{M}$ denote the internal forces and moments in the material form, respectively. $\boldsymbol{\Gamma}_N$ and $\boldsymbol{K}_M$ denote the material form of the axial and shear, and bending and torsional strain measures, respectively. $\widetilde{\boldsymbol{K}} = \mathbf{R}^{\mathsf{T}}\mathbf{R}_{,s}$ and $\widetilde{\boldsymbol{K}}_0 = \mathbf{R}_0^{\mathsf{T}}\mathbf{R}_{0,s}$ are the current and initial curvatures (skew-symmetric tensors) in the material form, respectively. $\mathbf{n}_0$ is the unit vector orthogonal to the beam cross section in the initial configuration. $\mathbf{R}_0 \in \text{SO}(3)$ is the rotation operator that expresses the rotation of the beam cross section in the initial configuration [57, 58].

2.3. Constitutive equations

We adopt a Saint Venant-Kirchhoff constitutive model. The material internal forces and couples are linearly related to the material strain measures as follows [31, 37, 48]

$$\boldsymbol{N} = \mathbb{C}_N\boldsymbol{\Gamma}_N \quad \text{and} \quad \boldsymbol{M} = \mathbb{C}_M\boldsymbol{K}_M\,, \tag{11}$$

with

$$\mathbb{C}_N = \text{diag}(GA_1, EA, GA_3) \quad \text{and} \quad \mathbb{C}_M = \text{diag}(EJ_1, GJ, EJ_3)\,, \tag{12}$$

where GA_1 and GA_3 are the shear stiffnesses along the cross section principal axes, EA is the axial stiffness; GJ is the torsional stiffness and EJ_1 and EJ_3 are the principal bending stiffnesses.

3. Time and space discretization of the governing equations

In this section we introduce the time and space discretized version of the governing equations and present the explicit Newmark time integration scheme with the associated geometrically consistent update procedure.

3.1. Time-discretized governing equations and configuration update

The right-hand sides of Eqs. (3) and (4) can be expressed in terms of kinematic quantities by exploiting the constitutive equations (11). Moreover, the local balance equations must be satisfied for each time $t = t^n$, leading to the following time-discretized version of the balance equations

$$\mu \boldsymbol{a}^n = \mathbf{R}^n \widetilde{\boldsymbol{K}}^n \mathbb{C}_N \boldsymbol{\Gamma}_N^n + \mathbf{R}^n \mathbb{C}_N \boldsymbol{\Gamma}_{N,s}^n + \bar{\boldsymbol{n}}^n \,, \tag{13}$$

$$\boldsymbol{j}^n \boldsymbol{\alpha}^n + \widetilde{\boldsymbol{\omega}}^n \boldsymbol{j}^n \boldsymbol{\omega}^n = \mathbf{R}^n \widetilde{\boldsymbol{K}}^n \mathbb{C}_M \boldsymbol{K}_M^n + \mathbf{R}^n \mathbb{C}_M \boldsymbol{K}_{M,s}^n + \boldsymbol{c}_{,s}^n \times \mathbf{R}^n \mathbb{C}_N \boldsymbol{\Gamma}_N^n + \bar{\boldsymbol{m}}^n \,, \tag{14}$$

where we denote with $()^n$ any quantity evaluated at time $t = t^n$. By revisiting in a time-discretized context the construction of the tangent space to the manifold $\mathcal{C}$ introduced with Eq. (2), see also [24], the configuration update from $\mathcal{C}^{(n-1)}$ to $\mathcal{C}^n$ is consistently performed as follows

$$\boldsymbol{c}^n = \boldsymbol{c}^{(n-1)} + \boldsymbol{\eta}^{(n-1)} \,, \tag{15}$$

$$\mathbf{R}^n = \exp(\widetilde{\boldsymbol{\vartheta}}^{(n-1)}) \mathbf{R}^{(n-1)} \,, \tag{16}$$

where $\boldsymbol{\eta}^{(n-1)} \in T_{\boldsymbol{c}^{(n-1)}} \boldsymbol{E}$ and $\widetilde{\boldsymbol{\vartheta}}^{(n-1)} \in \mathrm{so}(3)$ is such that $\widetilde{\boldsymbol{\vartheta}}^{(n-1)} \mathbf{R}^{(n-1)} \in T_{\mathbf{R}^{(n-1)}} \mathrm{SO}(3)$. $\boldsymbol{\eta}^{(n-1)}$ represents an incremental displacement field which acts (through a translation) on the configuration of the centroid line $\boldsymbol{c}^{(n-1)}$ and $\widetilde{\boldsymbol{\vartheta}}^{(n-1)}$ is an incremental spatial rotation field which acts (through the group composition) on the rotation $\mathbf{R}^{(n-1)}$. A sketch of the consistent time-stepping procedure is shown in Figure 2. The consistency of Eqs. (15) and (16) with the underlying geometric structure of the configuration manifold $\mathcal{C}$ is naturally guaranteed since the former is a standard translation in $\boldsymbol{E}$ and the latter complies with the group operation $\mathbf{R}^n = \exp(\widetilde{\boldsymbol{\vartheta}}^{(n-1)}) \mathbf{R}^{(n-1)}$, which represents a composition of two subsequent rotations whose result naturally remains on SO(3) [59]. This formulation crucially relies on the existence of an exact formula for the exponential map referred to as Rodrigues formula [59–62], given by

$$\exp(\widetilde{\boldsymbol{\psi}}) = \mathrm{id}_{\mathrm{SO}(3)} + \frac{\sin(\psi)}{\psi} \widetilde{\boldsymbol{\psi}} + \frac{1}{2} \left(\frac{\sin(\psi/2)}{\psi/2} \right)^2 \widetilde{\boldsymbol{\psi}}^2 \,, \tag{17}$$

where $\widetilde{\boldsymbol{\psi}}$ is the skew-symmetric matrix associated with a generic rotation vector $\boldsymbol{\psi}$ with modulus ψ.

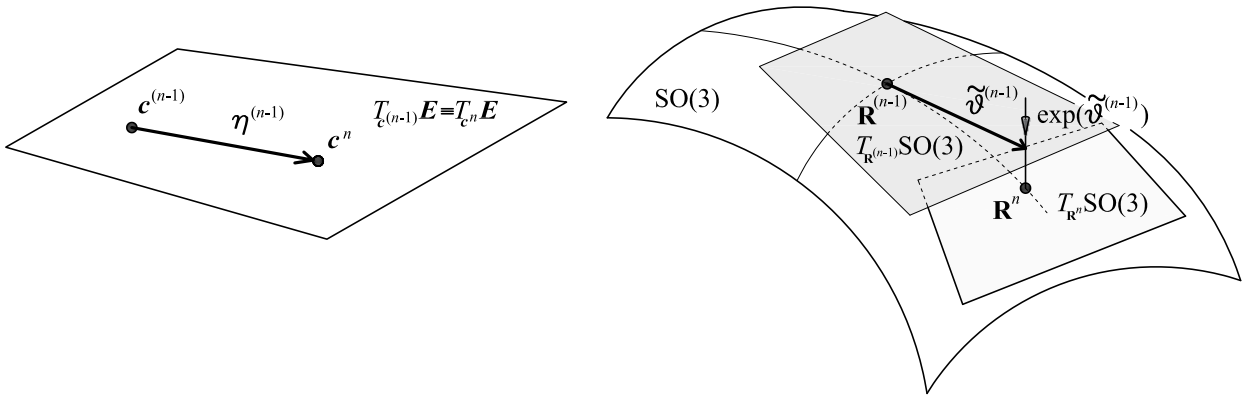

Figure 2: Sketch of the consistent configuration update: centroid position update (left) and rotation operator update (right).

3.2. Space discretization

With $\mathcal{I}_u = [u_0, u_{\mathrm{m}}] \subset \mathbb{R}$ as the normalized one-dimensional domain of the basis functions, the approximation of the variables is introduced as follows

$$\boldsymbol{c}(u) \approx \sum_{j=0}^{\mathrm{n}} R_{j,p}(u)\check{\boldsymbol{c}}_j \quad \text{with} \quad u \in \mathcal{I}_u\,, \tag{18}$$

$$\boldsymbol{\vartheta}(u) \approx \sum_{j=0}^{\mathrm{n}} R_{j,p}(u)\check{\boldsymbol{\vartheta}}_j \quad \text{with} \quad u \in \mathcal{I}_u\,, \tag{19}$$

$$\boldsymbol{\eta}(u) \approx \sum_{j=0}^{\mathrm{n}} R_{j,p}(u)\check{\boldsymbol{\eta}}_j \quad \text{with} \quad u \in \mathcal{I}_u\,, \tag{20}$$

$$\boldsymbol{\omega}(u) \approx \sum_{j=0}^{\mathrm{n}} R_{j,p}(u)\check{\boldsymbol{\omega}}_j \quad \text{with} \quad u \in \mathcal{I}_u\,, \tag{21}$$

$$\boldsymbol{v}(u) \approx \sum_{j=0}^{\mathrm{n}} R_{j,p}(u)\check{\boldsymbol{v}}_j \quad \text{with} \quad u \in \mathcal{I}_u\,, \tag{22}$$

$$\boldsymbol{\alpha}(u) \approx \sum_{j=0}^{\mathrm{n}} R_{j,p}(u)\check{\boldsymbol{\alpha}}_j \quad \text{with} \quad u \in \mathcal{I}_u\,, \tag{23}$$

$$\boldsymbol{a}(u) \approx \sum_{j=0}^{\mathrm{n}} R_{j,p}(u)\check{\boldsymbol{a}}_j \quad \text{with} \quad u \in \mathcal{I}_u\,, \tag{24}$$

where $\check{()}_j$ indicates the jth control value of the quantity; $R_{j,p}$ indicates the jth NURBS basis function of degree p [63]. We note that for convenience all the kinematic quantities are discretized in space, however, only $\check{\boldsymbol{\alpha}}_j$ and $\check{\boldsymbol{a}}_j$ are the primary variables of our problem.

3.3. Explicit Newmark scheme

At time $t = t^{n-1} = h(n-1)$, h being the time step size and n the time step counter, the control values of the incremental displacement and rotation vectors are expressed as follows

$$\check{\boldsymbol{\eta}}_j^{(n-1)} = h\check{\boldsymbol{v}}_j^{(n-1)} + \frac{h^2}{2}\,\check{\boldsymbol{a}}_j^{(n-1)}\,, \quad \text{with} \quad j = 0, \ldots, \mathrm{n}\,, \tag{25}$$

$$\check{\boldsymbol{\vartheta}}_j^{(n-1)} = h\check{\boldsymbol{\omega}}_j^{(n-1)} + \frac{h^2}{2}\,\check{\boldsymbol{\alpha}}_j^{(n-1)}\,, \quad \text{with} \quad j = 0, \ldots, \mathrm{n}\,. \tag{26}$$

The explicit central difference scheme is completed with the updating formulas for the velocities, which read as follows

$$\check{\boldsymbol{v}}_j^{n} = \check{\boldsymbol{v}}_j^{(n-1)} + \frac{h}{2}\,\left(\check{\boldsymbol{a}}_j^{(n-1)} + \check{\boldsymbol{a}}_j^{n}\right) = \check{\boldsymbol{v}}_{pj}^{(n-1)} + \frac{h}{2}\,\check{\boldsymbol{a}}_j^{n}\,, \tag{27}$$

$$\check{\boldsymbol{\omega}}_j^{n} = \check{\boldsymbol{\omega}}_j^{(n-1)} + \frac{h}{2}\,\left(\check{\boldsymbol{\alpha}}_j^{(n-1)} + \check{\boldsymbol{\alpha}}_j^{n}\right) = \check{\boldsymbol{\omega}}_{pj}^{(n-1)} + \frac{h}{2}\,\check{\boldsymbol{\alpha}}_j^{n}\,, \tag{28}$$

where we have defined $\check{\boldsymbol{v}}_{pj}^{(n-1)} = \check{\boldsymbol{v}}_j^{(n-1)} + \frac{h}{2}\,\check{\boldsymbol{a}}_j^{(n-1)}$ and $\check{\boldsymbol{\omega}}_{pj}^{(n-1)} = \check{\boldsymbol{\omega}}_j^{(n-1)} + \frac{h}{2}\,\check{\boldsymbol{\alpha}}_j^{(n-1)}$. We remark that apparently Eq. (28) is geometrically inconsistent since $\check{\boldsymbol{\alpha}}_j^{(n-1)}$ and $\check{\boldsymbol{\alpha}}_j^{n}$ belong to different tangent spaces, namely $T_{\mathbf{R}^{(n-1)}}\,\mathrm{SO}(3)$ and $T_{\mathbf{R}^{n}}\,\mathrm{SO}(3)$, respectively, and therefore could not be added. However, it has been demonstrated in [52] that for $\gamma = 1/2$, as in the present case, the projection $T_{\mathbf{R}^{(n-1)}}\,\mathrm{SO}(3) \to T_{\mathbf{R}^{n}}\,\mathrm{SO}(3)$ normally required to allow additive operations on $T_{\mathbf{R}^{n}}\,\mathrm{SO}(3)$ turns out to have no effects, so that Eq. (28) makes geometrically sense and takes the same form of Eq. (27).

3.4. Consistent update of the right hand sides of the governing equations

Eqs. (25) and (26) allow for a direct computation of the right hand sides of Eqs. (13) and (14), which contain quantities updated at time t^n. The updating procedure must be geometrically consistent with the configuration manifold, i.e. it must be developed consistently with Eqs. (15) and (16).

We start by updating the control points defining the beam axis

$$\check{\boldsymbol{c}}_j^{n} = \check{\boldsymbol{c}}_j^{(n-1)} + \check{\boldsymbol{\eta}}_j^{(n-1)} \quad \text{with} \quad j = 0, \ldots, \mathrm{n}\,, \tag{29}$$

from which we straightforwardly update the spatial configuration of the centroid line and its

derivatives

$$\boldsymbol{c}^n(u) = \sum_{j=0}^{n} R_{j,p}(u)\check{\boldsymbol{c}}_j^n\,, \tag{30}$$

$$\boldsymbol{c}^n{}_{,s}\,(u) = \sum_{j=0}^{n} R'_{j,p}(u)\check{\boldsymbol{c}}_j^n\,. \tag{31}$$

For the rotation variables we cannot use directly the exponential map since we only have updated control incremental rotations. We first compute the incremental rotation vector and its derivatives as follows

$$\boldsymbol{\vartheta}^{(n-1)}(u) = \sum_{j=0}^{\mathrm{n}} R_{j,p}(u)\check{\boldsymbol{\vartheta}}_j^{(n-1)}\,, \tag{32}$$

$$\boldsymbol{\vartheta}_{,s}^{(n-1)}\,(u) = \sum_{j=0}^{\mathrm{n}} R'_{j,p}(u)\check{\boldsymbol{\vartheta}}_j^{(n-1)}\,, \tag{33}$$

$$\boldsymbol{\vartheta}_{,ss}^{(n-1)}\,(u) = \sum_{j=0}^{\mathrm{n}} R''_{j,p}(u)\check{\boldsymbol{\vartheta}}_j^{(n-1)}\,, \tag{34}$$

and then, by using Eq.(16), the rotation operator is consistently updated at time t^n as follows

$$\mathbf{R}^n(u) = \exp(\widetilde{\boldsymbol{\vartheta}}^{(n-1)}(u))\mathbf{R}^{(n-1)}(u)\,. \tag{35}$$

Once the rotation operator is updated, the spatial inertia tensor is straightforwardly updated as follows

$$\boldsymbol{j}^n(u) = \mathbf{R}^n(u)\boldsymbol{J}(u)\mathbf{R}^{\mathsf{T}n}(u)\,. \tag{36}$$

By exploiting the updating formulas proposed in [24], the strain measures and their derivatives are updated as shown in the following.

Update of the curvature tensor and its derivative.

$$\widetilde{\boldsymbol{K}}^n = \widetilde{\boldsymbol{K}}^{(n-1)} + \mathbf{R}^{\mathsf{T}(n-1)}(d\exp_{\widetilde{\boldsymbol{\vartheta}}}\widetilde{\boldsymbol{\vartheta}}_{,s}^{(n-1)})\mathbf{R}^{(n-1)}\,. \tag{37}$$

$$\begin{aligned}\widetilde{\boldsymbol{K}}_{,s}^{\,n} = \widetilde{\boldsymbol{K}}_{,s}^{(n-1)} - \widetilde{\boldsymbol{K}}^{(n-1)}\mathbf{R}^{\mathsf{T}(n-1)}(d\exp_{\widetilde{\boldsymbol{\vartheta}}}\widetilde{\boldsymbol{\vartheta}}_{,s}^{(n-1)})\mathbf{R}^{(n-1)} \\ +\mathbf{R}^{\mathsf{T}(n-1)}(d\exp_{\widetilde{\boldsymbol{\vartheta}}}\widetilde{\boldsymbol{\vartheta}}_{,s}^{(n-1)})\mathbf{R}^{(n-1)}\widetilde{\boldsymbol{K}}^{(n-1)} + \mathbf{R}^{\mathsf{T}(n-1)}(d\exp_{\widetilde{\boldsymbol{\vartheta}}}\widetilde{\boldsymbol{\vartheta}}_{,s}^{(n-1)})_{,s}\,\mathbf{R}^{(n-1)}\,,\end{aligned} \tag{38}$$

from which $\boldsymbol{K}_{M,s}^n = \boldsymbol{K}_{,s}^n - \boldsymbol{K}_{0,s}$ can be computed.

Eqs. (37) and (38) require the evaluation of the first and second derivatives of the exponential map, namely $d\exp_{\widetilde{\boldsymbol{\vartheta}}}\widetilde{\boldsymbol{\vartheta}}_{,s}^{(n-1)}$ and its derivative with respect to s. As done in [24], this is accomplished by means of a series [64], in which, due to the very small time steps, only terms up to the third-order are considered.

Update of the shear and axial strain measure vector and its derivatives.

$$\boldsymbol{\Gamma}_N^n = \mathbf{R}^{\mathsf{T}n}\boldsymbol{c}_{,s}^{\,n} - \mathbf{R}_0^{\mathsf{T}}\mathbf{n}_0\,. \tag{39}$$

By making use of the updated curvature vector, we have

$$\boldsymbol{\Gamma}_{N,s}^n = -\widetilde{\boldsymbol{K}}^n\mathbf{R}^{\mathsf{T}n}\boldsymbol{c}_{,s}^{\,n} + \mathbf{R}^{\mathsf{T}n}\boldsymbol{c}_{,ss}^{\,n} + \widetilde{\boldsymbol{K}}_0\mathbf{R}_0^{\mathsf{T}}\boldsymbol{c}_{0,s} - \mathbf{R}_0^{\mathsf{T}}\boldsymbol{c}_{0,ss}\,. \tag{40}$$

where $\boldsymbol{c}_0$ is the centroid line in the initial configuration.

For additional details on the above update formulas we refer to [24, 27].

4. Solution method

In this section we collocate the balance equations and present the details of the solution procedure which involves the linearization of the rotational balance equation.

4.1. Collocated balance equations

In recent studies [9, 15, 65, 66] alternative choices for collocation have been proposed to achieve optimal convergence rates, however, in this work the equations are collocated at the standard Greville abscissae [1] leaving to future developments the study of different choices of collocation points. Note that sometimes in the following a quantity evaluated at the ith collocation point u_i^c is indicated simply with a subscript i.

With Eqs. (30), (31), (35), (36), (37), (38), (39) and (40) the right hand sides of Eqs. (13) and (14) become known quantities. At the ith collocation point the balance equations can be rewritten in a more compact form as follows

$$\mu\boldsymbol{a}_i^n = \boldsymbol{\psi}_i^n \quad \text{with} \quad i = 1,\ldots,\mathrm{n}-1\,, \tag{41}$$

$$\boldsymbol{j}_i^n\boldsymbol{\alpha}_i^n + \widetilde{\boldsymbol{\omega}}_i^n\boldsymbol{j}_i^n\boldsymbol{\omega}_i^n = \boldsymbol{\chi}_i^n \quad \text{with} \quad i = 1,\ldots,\mathrm{n}-1\,, \tag{42}$$

where we have set

$$\boldsymbol{\psi}_i^n = \left[\mathbf{R}^n\widetilde{\boldsymbol{K}}^n\mathbb{C}_N\boldsymbol{\Gamma}_N^n + \mathbf{R}^n\mathbb{C}_N\boldsymbol{\Gamma}_{N,s}^n + \bar{\boldsymbol{n}}^n\right]_{u=u_i^c}, \tag{43}$$

$$\boldsymbol{\chi}_i^n = \left[\mathbf{R}^n\widetilde{\boldsymbol{K}}^n\mathbb{C}_M\boldsymbol{K}_M^n + \mathbf{R}^n\mathbb{C}_M\boldsymbol{K}_{M,s}^n + \boldsymbol{c}_{,s}^n\times\mathbf{R}^n\mathbb{C}_N\boldsymbol{\Gamma}_N^n + \bar{\boldsymbol{m}}^n\right]_{u=u_i^c}. \tag{44}$$

4.2. Solution procedure

The primary unknowns of our problem are the control values of angular and linear accelerations $\check{\boldsymbol{\alpha}}_j^n$ and $\check{\boldsymbol{a}}_j^n$ with $j = 0,\dots,\mathrm{n}$. In contrast to the collocated translational balance equations (Eq. (41)) that can be discretized in space straightforwardly as follows

$$\mu\sum_{j=0}^{\mathrm{n}} R_j(u_i^c)\check{\boldsymbol{a}}_j^n = \boldsymbol{\psi}_i^n \quad \text{with} \quad i = 1,\dots,\mathrm{n}-1\,, \tag{45}$$

the collocated rotational balance equations (Eq. (42)) turn out to be nonlinear with respect to $\boldsymbol{\alpha}_i^n$. This is seen by substituting Eq. (28) into Eq. (42) leading to

$$\boldsymbol{j}_i^n\boldsymbol{\alpha}_i^n + \left[\boldsymbol{\omega}_{p,i}^{(n-1)} + \frac{h}{2}\boldsymbol{\alpha}_i^n\right]\times\boldsymbol{j}^n\left[\boldsymbol{\omega}_{p,i}^{(n-1)} + \frac{h}{2}\boldsymbol{\alpha}_i^n\right] = \boldsymbol{\chi}_i^n \quad \text{with} \quad i = 1,\dots,\mathrm{n}-1\,. \tag{46}$$

The presence of the nonlinear term in the time-discretized rotational balance equation raises the need for a Newton-Raphson scheme where the linearized version of the rotational balance equation is used. By revisiting in the IGA-C context the procedure used in [52] for rigid bodies, we rewrite the ith nonlinear equation in a residual form as follows

$$\mathbf{r}_i^n(\boldsymbol{\alpha}_i^n) = \boldsymbol{j}_i^n\boldsymbol{\alpha}_i^n + \left[\boldsymbol{\omega}_{p,i}^{(n-1)} + \frac{h}{2}\boldsymbol{\alpha}_i^n\right]\times\boldsymbol{j}^n\left[\boldsymbol{\omega}_{p,i}^{(n-1)} + \frac{h}{2}\boldsymbol{\alpha}_i^n\right] - \boldsymbol{\chi}_i^n = \mathbf{0} \quad \text{with} \quad i = 1,\dots,\mathrm{n}-1\,, \tag{47}$$

whose linearized version is given by

$$L[\mathbf{r}_i^n(\boldsymbol{\alpha}_i^n)] = \hat{\mathbf{r}}_i^n + \frac{\partial\mathbf{r}_i^n(\hat{\boldsymbol{\alpha}}_i^n)}{\partial\boldsymbol{\alpha}_i^n}\Delta\boldsymbol{\alpha}_i^n = \mathbf{0}\,, \tag{48}$$

where $\hat{()}$ indicates a quantity evaluated at the current iteration, while $\Delta\boldsymbol{\alpha}_i^n$ is the increment of the angular acceleration at the ith collocation point. The tangent operator appearing in Eq. (48) is given by

$$\frac{\partial\mathbf{r}_i^n(\hat{\boldsymbol{\alpha}}_i^n)}{\partial\boldsymbol{\alpha}_i^n} = \boldsymbol{j}_i^n + \frac{h}{2}\left(\widetilde{\boldsymbol{\omega}}_{p,i}^{(n-1)}\boldsymbol{j}_i^n - \widetilde{\boldsymbol{j}_i^n\boldsymbol{\omega}_{p,i}^{(n-1)}}\right) + \frac{h^2}{4}\left(\widetilde{\hat{\boldsymbol{\alpha}}}_i^n\boldsymbol{j}_i^n - \widetilde{\boldsymbol{j}_i^n\hat{\boldsymbol{\alpha}}_i^n}\right). \tag{49}$$

Finally, the linearized and spatially discretized version of Eq. (46) becomes

$$\frac{\partial \mathbf{r}_i^n(\hat{\boldsymbol{\alpha}}_i^n)}{\partial \boldsymbol{\alpha}_i^n} \sum_{j=0}^{\mathrm{n}} R_j(u_i^c) \Delta \check{\boldsymbol{\alpha}}_j^n = -\hat{\mathbf{r}}_i^n \quad \text{with} \quad i = 1, \ldots, \mathrm{n}-1\,. \tag{50}$$

Eqs. (41) and (42) need to be completed with four boundary conditions which are discussed in the following.

4.3. Dirichlet boundary conditions

The discretized and collocated form of Dirichlet boundary conditions, see Eqs. (5) and (6), is

$$\boldsymbol{\eta}_i^n = \sum_{j=0}^{\mathrm{n}} R_j(u_i^c) \check{\boldsymbol{\eta}}_j^n = \bar{\boldsymbol{\eta}}_c^n\,, \tag{51}$$

$$\boldsymbol{\vartheta}_i^n = \sum_{j=0}^{\mathrm{n}} R_j(u_i^c) \check{\boldsymbol{\vartheta}}_j^n = \bar{\boldsymbol{\vartheta}}_c^n\,, \tag{52}$$

where $i = 0$ and/or n. Without loss of generality, we consider the case of a clamped end for which $\bar{\boldsymbol{\eta}}_c^n = \bar{\boldsymbol{\vartheta}}_c^n = 0$, for each time instant t^n. In this case, Eqs. (51) and (52), by making use of Eqs. (25)-(28) and recalling that NURBS basis functions interpolate the boundary values, become

$$\check{\boldsymbol{a}}_j^n = -\frac{1}{h}\, \check{\boldsymbol{v}}_{pj}^{(n-1)}\,, \tag{53}$$

$$\check{\boldsymbol{\alpha}}_j^n = -\frac{1}{h}\, \check{\boldsymbol{\omega}}_{pj}^{(n-1)}\,, \tag{54}$$

where $j = 0$ or n, depending on which end of the beam is considered.

4.4. Neumann boundary conditions

The Neumann boundary conditions, see Eqs. (5) and (6), need firstly to be linearized in order to be expressed in terms of our primary variables. Following the procedure discussed in [24, 27], the linearized form is given by

$$\left[\hat{\mathbf{R}}\mathbb{C}_N\hat{\mathbf{R}}^{\mathsf{T}}\hat{\tilde{c}}_{,s} - \widetilde{\left(\hat{\mathbf{R}}\mathbb{C}_N\hat{\boldsymbol{\Gamma}}_N\right)}\right]\boldsymbol{\vartheta} + \left[\hat{\mathbf{R}}\mathbb{C}_N\hat{\mathbf{R}}^{\mathsf{T}}\right]\boldsymbol{\eta}_{,s} = -\left(\hat{\mathbf{R}}\mathbb{C}_N\hat{\boldsymbol{\Gamma}}_N - \bar{\boldsymbol{n}}_c\right)\,, \tag{55}$$

$$\left[-\widetilde{\left(\hat{\mathbf{R}}\mathbb{C}_M\hat{\boldsymbol{K}}_M\right)}\right]\boldsymbol{\vartheta} + \left[\hat{\mathbf{R}}\mathbb{C}_M\hat{\mathbf{R}}^{\mathsf{T}}\right]\boldsymbol{\vartheta}_{,s} = -\left(\hat{\mathbf{R}}\mathbb{C}_M\hat{\boldsymbol{K}}_M - \bar{\boldsymbol{m}}_c\right)\,. \tag{56}$$

The collocated and discretized (both in space and time) versions of the above equations become

$$ {}^{1}\boldsymbol{\psi}_i^n \sum_{j=0}^{\mathrm{n}} R_{j,p}(u_i^c)\check{\boldsymbol{\vartheta}}_j^n + {}^{2}\boldsymbol{\psi}_i^n \sum_{j=0}^{\mathrm{n}} R'_{j,p}(u_i^c)\check{\boldsymbol{\eta}}_j^n = \bar{\boldsymbol{\psi}}_i^n \,, \tag{57} $$

$$ {}^{1}\boldsymbol{\chi}_i^n \sum_{j=0}^{\mathrm{n}} R_{j,p}(u_i^c)\check{\boldsymbol{\vartheta}}_j^n + {}^{2}\boldsymbol{\chi}_i^n \sum_{j=0}^{\mathrm{n}} R'_{j,p}(u_i^c)\check{\boldsymbol{\vartheta}}_j^n = \bar{\boldsymbol{\chi}}_i^n \,, \tag{58} $$

where we have set

$$ {}^{1}\boldsymbol{\psi}_i^n = \left[\hat{\mathbf{R}}^n \mathbb{C}_N \hat{\mathbf{R}}^{\mathsf{T}n} \hat{\widetilde{\boldsymbol{c}}}_{,s}^{\,n} - \left(\widetilde{\hat{\mathbf{R}}^n \mathbb{C}_N \hat{\boldsymbol{\Gamma}}_N^n} \right) \right]_{u=u_i^c} , \tag{59} $$

$$ {}^{2}\boldsymbol{\psi}_i^n = \left[\hat{\mathbf{R}}^n \mathbb{C}_N \hat{\mathbf{R}}^{\mathsf{T}n} \right]_{u=u_i^c} , \tag{60} $$

$$ {}^{1}\boldsymbol{\chi}_i^n = \left[-\left(\widetilde{\hat{\mathbf{R}}^n \mathbb{C}_M \hat{\boldsymbol{K}}_M^n} \right) \right]_{u=u_i^c} , \tag{61} $$

$$ {}^{2}\boldsymbol{\chi}_i^n = \left[\hat{\mathbf{R}}^n \mathbb{C}_M \hat{\mathbf{R}}^{\mathsf{T}n} \right]_{u=u_i^c} , \tag{62} $$

$$ \bar{\boldsymbol{\psi}}_i^n = -\left(\hat{\mathbf{R}}^n \mathbb{C}_N \hat{\boldsymbol{\Gamma}}_N^n - \bar{\boldsymbol{n}}_c^n \right)_{u=u_i^c} , \tag{63} $$

$$ \bar{\boldsymbol{\chi}}_i^n = -\left(\hat{\mathbf{R}}^n \mathbb{C}_M \hat{\boldsymbol{K}}_M^n - \bar{\boldsymbol{m}}_c^n \right)_{u=u_i^c} , \tag{64} $$

where $i = 0$ or n, depending on which end of the beam is considered.

The combination of Eqs. (25) and (26) with (27) and (28) evaluated at time t^n instead of $t^{(n-1)}$, permits expressing the incremental displacements and rotations as follows

$$ \check{\boldsymbol{\eta}}_j^n = h\check{\boldsymbol{v}}_{pj}^{(n-1)} + h^2 \check{\boldsymbol{a}}_j^n \,, \quad \text{with} \quad j = 0, \ldots, \mathrm{n} \,, \tag{65} $$

$$ \check{\boldsymbol{\vartheta}}_j^n = h\check{\boldsymbol{\omega}}_{pj}^{(n-1)} + h^2 \check{\boldsymbol{\alpha}}_j^n \,, \quad \text{with} \quad j = 0, \ldots, \mathrm{n} \,. \tag{66} $$

Eqs. (65) and (66) are finally replaced into Eqs. (57) and (58) to obtain the boundary conditions in terms of the primary unknowns $\check{\boldsymbol{\alpha}}_j^n$ and $\check{\boldsymbol{a}}_j^n$ as follows

$$ {}^{1}\boldsymbol{\psi}_i^n h^2 \sum_{j=0}^{\mathrm{n}} R_{j,p}\check{\boldsymbol{\alpha}}_j^n + {}^{2}\boldsymbol{\psi}_i^n h^2 \sum_{j=0}^{\mathrm{n}} R'_{j,p}\check{\boldsymbol{a}}_j^n = \bar{\boldsymbol{\psi}}_i^n - h\left({}^{1}\boldsymbol{\psi}_i^n \sum_{j=0}^{\mathrm{n}} R_{j,p}\check{\boldsymbol{\omega}}_{pj}^{(n-1)} + {}^{2}\boldsymbol{\psi}_i^n \sum_{j=0}^{\mathrm{n}} R'_{j,p}\check{\boldsymbol{v}}_{pj}^{(n-1)} \right) , \tag{67} $$

$$ h^2 \left({}^{1}\boldsymbol{\chi}_i^n \sum_{j=0}^{\mathrm{n}} R_{j,p} + {}^{2}\boldsymbol{\chi}_i^n \sum_{j=0}^{n} R'_{j,p} \right) \check{\boldsymbol{\alpha}}_j^n = \bar{\boldsymbol{\chi}}_i^n - h\left({}^{1}\boldsymbol{\chi}_i^n \sum_{j=0}^{\mathrm{n}} R_{j,p} + {}^{2}\boldsymbol{\chi}_i^n \sum_{j=0}^{\mathrm{n}} R'_{j,p} \right) \check{\boldsymbol{\omega}}_{pj}^{(n-1)} \,. \tag{68} $$

We note that the translational equation (Eq. (67)) gives rise to a coupling between the linear and angular accelerations.

4.5. Initial conditions

Linear and angular accelerations at the initial time are unknown since only linear and angular velocities are normally assigned. Here we present the procedure we employed to calculate initial accelerations.

4.5.1. Internal collocation points

The governing equations at the initial time read

$$\mu \boldsymbol{a}_i^0 = \boldsymbol{\psi}_i^0 \quad \text{with} \quad i = 1, \dots, \mathrm{n}-1\,, \tag{69}$$

$$\boldsymbol{j}_i^0 \boldsymbol{\alpha}_i^0 + \widetilde{\boldsymbol{\omega}}_i^0 \boldsymbol{j}^0 \boldsymbol{\omega}_i^0 = \boldsymbol{\chi}_i^0 \quad \text{with} \quad i = 1, \dots, \mathrm{n}-1\,, \tag{70}$$

from which we obtain

$$\mu \sum_{j=0}^{\mathrm{n}} R_j(u_i^c) \check{\boldsymbol{a}}_j^0 = \boldsymbol{\psi}_i^0 \quad \text{with} \quad i = 1, \dots, \mathrm{n}-1\,, \tag{71}$$

$$\sum_{j=0}^{\mathrm{n}} R_j(u_i^c) \check{\boldsymbol{\alpha}}_j^0 = \left(\boldsymbol{j}_i^0\right)^{-1} \left(\boldsymbol{\chi}_i^0 - \widetilde{\boldsymbol{\omega}}_i^0 \boldsymbol{j}_i^0 \boldsymbol{\omega}_i^0\right) \quad \text{with} \quad i = 1, \dots, \mathrm{n}-1\,, \tag{72}$$

where $\boldsymbol{\psi}_i^0$ and $\boldsymbol{\chi}_i^0$ are given by Eqs. (43) and (44) evaluated at $t = t^0$.

4.5.2. Dirichlet boundary conditions

Consider for example the case of a clamped end. The initial boundary conditions are

$$\boldsymbol{\eta}_i^0 = \sum_{j=0}^{\mathrm{n}} R_j(u_i^c) \check{\boldsymbol{\eta}}_j^0 = 0\,, \tag{73}$$

$$\boldsymbol{\vartheta}_i^0 = \sum_{j=0}^{\mathrm{n}} R_j(u_i^c) \check{\boldsymbol{\vartheta}}_j^0 = 0\,, \tag{74}$$

where $i = 0$ or n depending on which end of the beam is considered. Eqs. (73) and (74), by making use of Eqs. (25) and (26) evaluated at $t = t^0$, become

$$\sum_{j=0}^{\mathrm{n}} R_j(u_i^c) \check{\boldsymbol{a}}_j^0 = -\frac{2}{h} \sum_{j=0}^{\mathrm{n}} R_j(u_i^c) \check{\boldsymbol{v}}_j^0\,, \tag{75}$$

$$\sum_{j=0}^{\mathrm{n}} R_j(u_i^c) \check{\boldsymbol{\alpha}}_j^0 = -\frac{2}{h} \sum_{j=0}^{\mathrm{n}} R_j(u_i^c) \check{\boldsymbol{\omega}}_j^0\,. \tag{76}$$

4.5.3. Neumann boundary conditions

Again by replacing Eqs. (25) and (26) evaluated at $t = t^0$ into Eqs. (57) and (58) we obtain the boundary conditions in terms of the primary unknowns $\check{\boldsymbol{\alpha}}_j^0$ and $\check{\boldsymbol{a}}_j^0$

$$ {}^1\boldsymbol{\psi}_i^0 \sum_{j=0}^{\mathrm{n}} R_{j,p} \frac{h^2}{2} \check{\boldsymbol{\alpha}}_j^0 + {}^2\boldsymbol{\psi}_i^0 \sum_{j=0}^{\mathrm{n}} R'_{j,p} \frac{h^2}{2} \check{\boldsymbol{a}}_j^0 = \bar{\boldsymbol{\psi}}_i^0 - h \left({}^1\boldsymbol{\psi}_i^0 \sum_{j=0}^{\mathrm{n}} R_{j,p} \check{\boldsymbol{\omega}}_j^0 + {}^2\boldsymbol{\psi}_i^0 \sum_{j=0}^{\mathrm{n}} R'_{j,p} \check{\boldsymbol{v}}_j^0 \right) , \quad (77) $$

$$ \left({}^1\boldsymbol{\chi}_i^0 \sum_{j=0}^{n} R_{j,p} + {}^2\boldsymbol{\chi}_i^0 \sum_{j=0}^{n} R'_{j,p} \right) \frac{h^2}{2} \check{\boldsymbol{\alpha}}_j^0 = \bar{\boldsymbol{\chi}}_i^0 - h \left({}^1\boldsymbol{\chi}_i^0 \sum_{j=0}^{n} R_{j,p} + {}^2\boldsymbol{\chi}_i^0 \sum_{j=0}^{n} R'_{j,p} \right) \check{\boldsymbol{\omega}}_j^0 , \quad (78) $$

where $i = 0$ or n depending on which end of the beam is considered and ${}^1\boldsymbol{\psi}_i^0$, ${}^2\boldsymbol{\psi}_i^0$, ${}^1\boldsymbol{\chi}_i^0$, ${}^2\boldsymbol{\chi}_i^0$, $\bar{\boldsymbol{\psi}}_i^0$, $\bar{\boldsymbol{\chi}}_i^0$ are the same as in Eqs. (59)-(64) but evaluated at $t = t^0$.

5. Numerical results and discussion

In this section we present the results of some numerical applications selected to test the capabilities of the formulation when fast and very large motions occur and different boundary conditions are imposed.

5.1. Cantilever beam

In the first numerical application we consider a simple cantilever beam, similar to the one analyzed in [67], with length $L = 1\,\mathrm{m}$ and square cross section with side 0.01 m. The Young's modulus is $E = 210 \times 10^9\,\mathrm{N/m^2}$, the Poisson's ratio is $\nu = 0.2$ and material density is $\rho = 7800\,\mathrm{kg/m^3}$. Initially the beam axis is placed along x_2 and the deformation occurs in the (x_2, x_3) plane. A concentrated downward (negative) transversal tip force F_3, constant in time, is applied impulsively. In Figure 3 the time histories of the beam tip displacements are shown. We consider two load intensities: $F_3 = -10\,\mathrm{N}$ (the same as in [67]) and $F_3 = -100\,\mathrm{N}$. For both cases $p = 4$, $n = 20$ and a time step $h = 1 \times 10^{-6}\,\mathrm{s}$ is used. An excellent agreement is found with the results obtained by Gravouil & Comberscure in [67]. In Figure 4 four snapshots of the deformed beam are shown. For both loads, identical time histories are obtained with a halved time step $h = 5 \times 10^{-7}\,\mathrm{s}$. To assess the higher-order space-accuracy of the method when fast and large motions occur, in Figure 5 we show the convergence curves of the L_2 norm of the error for the load case $F_3 = -100\,\mathrm{N}$. The error is calculated as $err_{L_2} = ||\boldsymbol{u}^r - \boldsymbol{u}^h||_{L_2} / ||\boldsymbol{u}^r||_{L_2}$, where $\boldsymbol{u}^h$ and $\boldsymbol{u}^r$ are the approximate and reference vertical

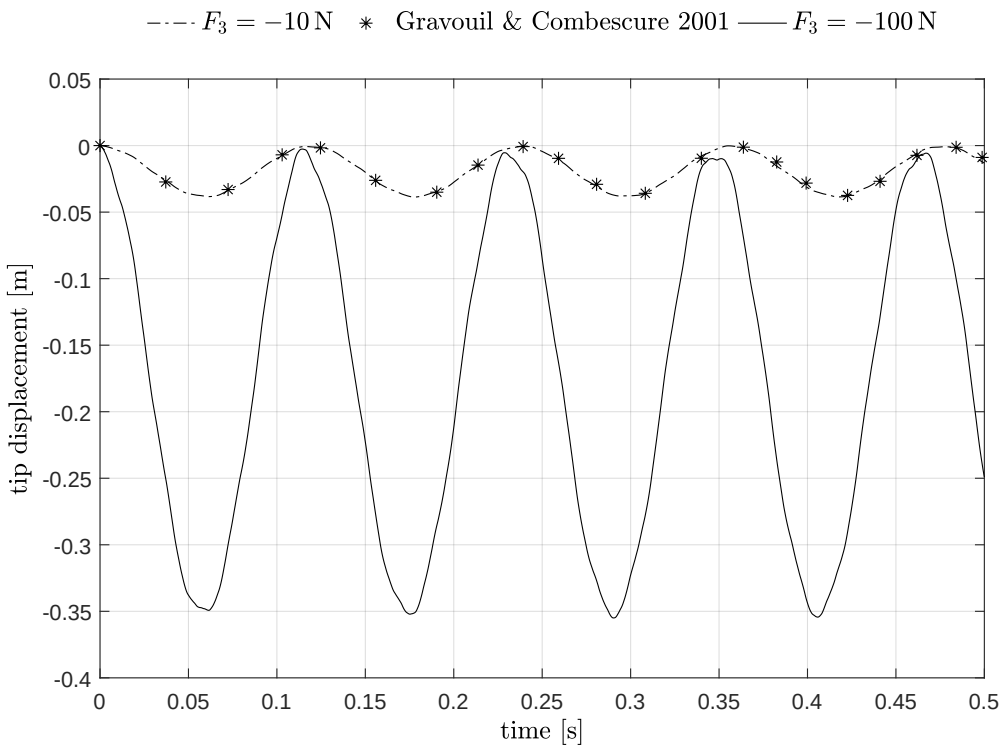

Figure 3: Tip displacement of a cantilever beam subjected to a tip transversal load F_3 with two different intensities: $-10\,\mathrm{N}$ (dash-dot line), compared with the solution obtained in [67] ($*$), and $-100\,\mathrm{N}$ (solid line). For both cases $p = 4$, $n = 20$, $h = 1 \times 10^{-6}$.

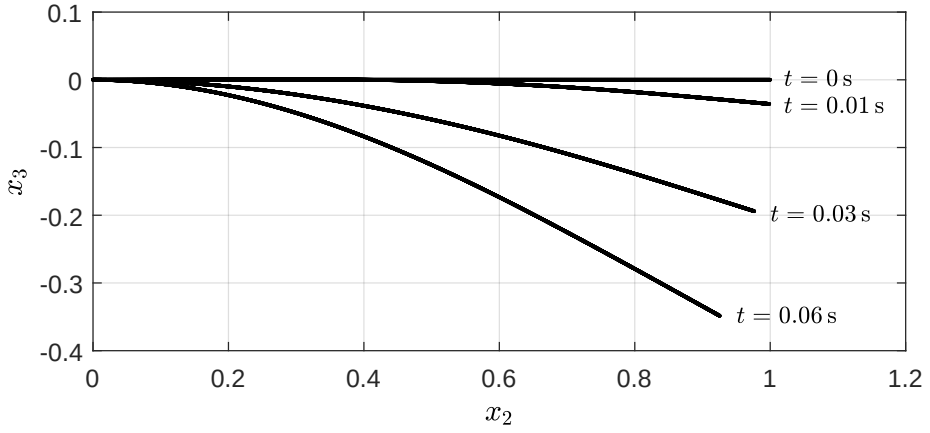

Figure 4: Snapshots of a cantilever beam subjected to a tip force $F_3 = -100\,\mathrm{N}$. $p = 4$, $n = 20, h = 1 \times 10^{-6}\,\mathrm{s}$.

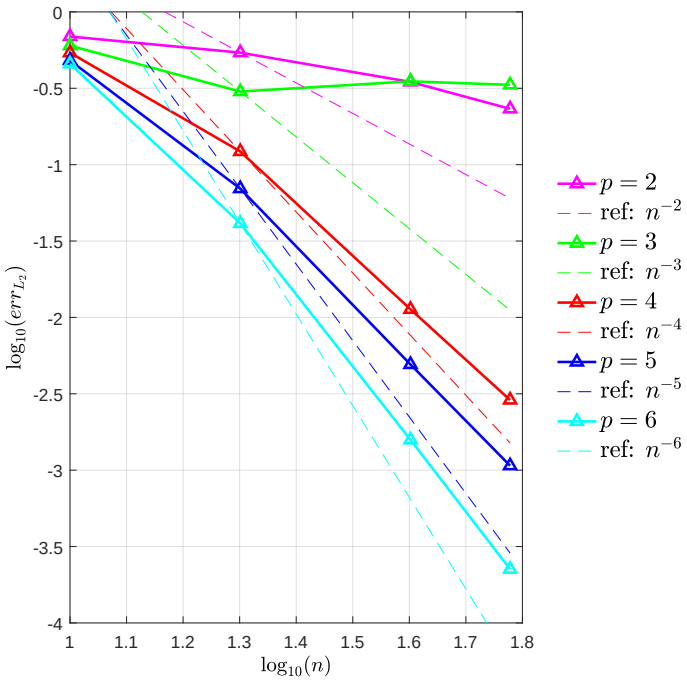

Figure 5: L_2 norm of error vs. number of collocation points for a cantilever beam under an in-plane transversal tip force with NURBS basis functions of degrees $p = 2, \ldots, 6$. Dashed lines indicate reference orders of convergence.

displacements, respectively, evaluated at $t = 1\,\text{ms}$. The reference solution $\boldsymbol{u}^r$ is obtained with $p = 6$, $n = 80$ and a time step $h = 1 \times 10^{-7}\,\text{s}$. In this convergence study, the critical time step size for all combinations of n and p is estimated using the ratio between the average element size, approximated by $L/(np)$, and the bar-wave velocity $\sqrt{E/\rho}$ [68]. Time step sizes, preliminary assessed in this way, are further reduced in order to make sure that the spatial error dominates the temporal one so to capture the effects of spatial refinement. In the end, the following time steps are used: 1×10^{-6}, 0.5×10^{-6}, 0.25×10^{-6}, $0.125 \times 10^{-6}\,\text{s}$ for $n = 10$, 20, 40, 60, respectively, regardless of the approximation degree p. Figure 5 shows convergence rates of order p, apart from the low-order cases (especially for $p = 3$), which perform poorly also in the static displacement-based formulations due to locking effects as documented in [24, 27].

Finally, we observe that the presence of the nonlinear term in the rotational balance equation has a negligible impact on the overall efficiency of the method since the Newton-

Raphson iterative scheme converges always in one iteration (with a tolerance of 10^{-10} on the maximum value of the residual) regardless of the amplitude and velocity of the motion. This is due to the fact that the stability condition for the explicit method requires such a small time step that the nonlinearity associated with the angular velocity is very weak.

5.2. Swinging flexible pendulum

The second numerical test is the swinging flexible pendulum. It consists of an initially horizontal beam of length L with its axis laying along x_2 hinged at the end located at $(0, 0, 0)$ and free at the other end initially located at $(0, L, 0)$. Once released, the beam falls down under the effect of gravity. Similar examples are proposed in [28, 39, 69, 70], where implicit solvers are used. We repeat here with our explicit method the same test proposed in [28, 39]. We consider a beam of length $L = 1\,\mathrm{m}$ with circular cross section with diameter $0.01\,\mathrm{m}$. The Young's modulus is $E = 5 \times 10^6\,\mathrm{N/m^2}$, the Poisson's ratio is $\nu = 0.5$ and the material density is $\rho = 1100\,\mathrm{kg/m^3}$. The spatial approximation is made with basis functions of degree $p = 4$ and $n = 30$. The simulation time is $1\,\mathrm{s}$ and we use a time step size $h = 1 \times 10^{-5}\,\mathrm{s}$. Unlike in the previous numerical application, where a very stiff beam is considered, in this case the beam has a much higher flexibility. Moreover, due to the hinged end, this test is used to verify the reliability of our formulation when mixed Dirichlet–Neumann boundary conditions are assigned. Figure 6 shows some snapshots taken from time 0 to $1\,\mathrm{s}$ with increments of $0.1\,\mathrm{s}$. The time history of the tip displacement is shown in Figure 7. An excellent agreement with the results obtained in [28, 39] is found.

5.3. Three-dimensional flying beam

This example was proposed for the first time by Simo & Vu-Quoc in [30] and later studied also in [41, 71, 72]. The test consists of an initially straight free flexible beam placed in the plane (x_2, x_3). At the lower end three different time-varying concentrated loads are applied simultaneously, namely: a positive force F_2 applied along x_2, and a torque with a negative component M_1 along x_1 and a positive component M_3 along x_3, see Figure 8(a). At time 2.5 the three loads reach their maxim values, which are 20, 200 and 100, respectively. The time histories of these loads are shown in Figure 8(b).

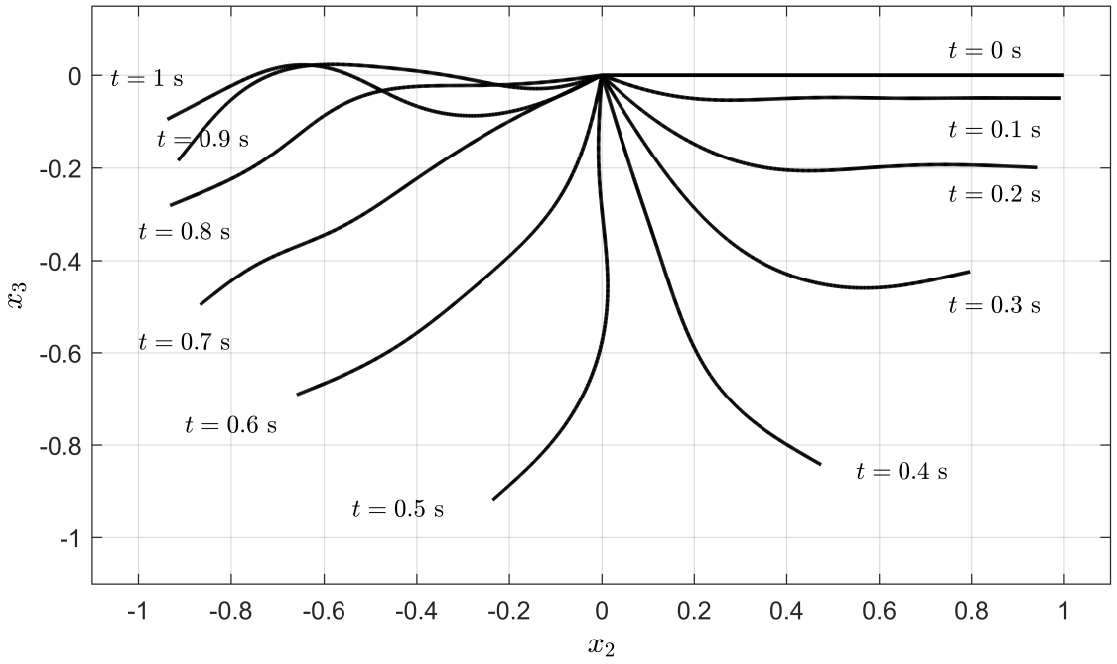

Figure 6: Snapshots of a swinging flexible pendulum from time 0 to 1 s with increments of 0.1 s. $p = 4$, $n = 30$, $h = 1 \times 10^{-5}$ s.

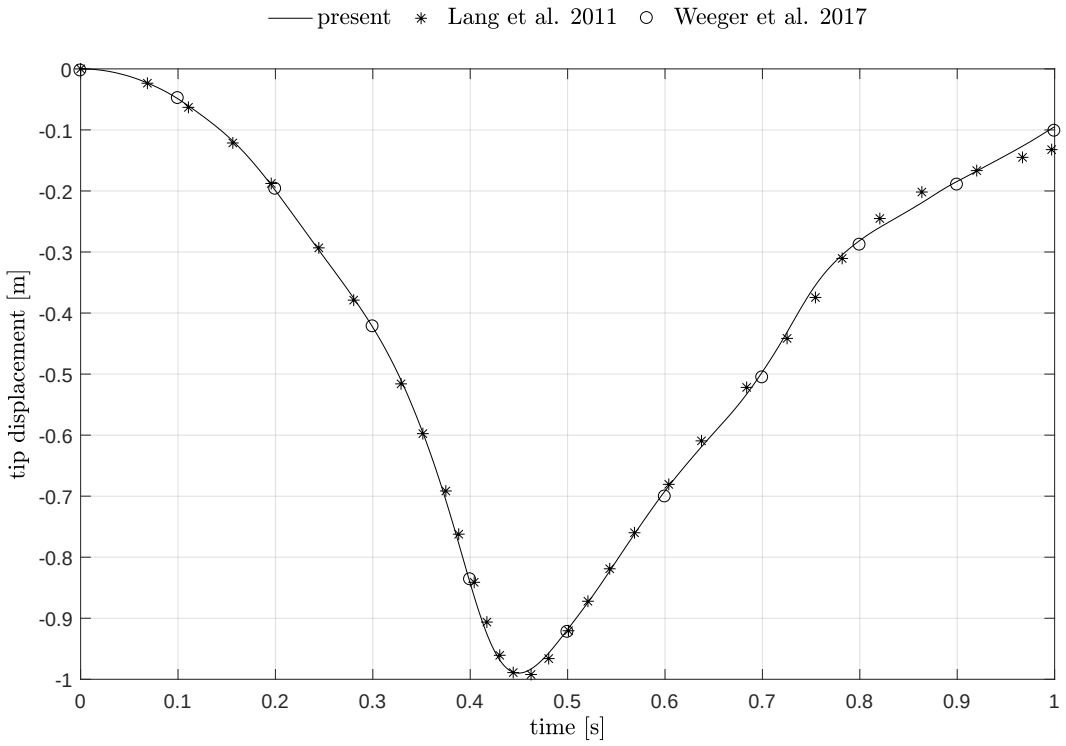

Figure 7: Vertical tip displacement of a swinging flexible pendulum: comparison of the present case for $p = 4$, $n = 30$, $h = 1 \times 10^{-5}$ s (solid line) with Lang et al. [39] ($*$) and Weeger et al. [28] ($\circ$).

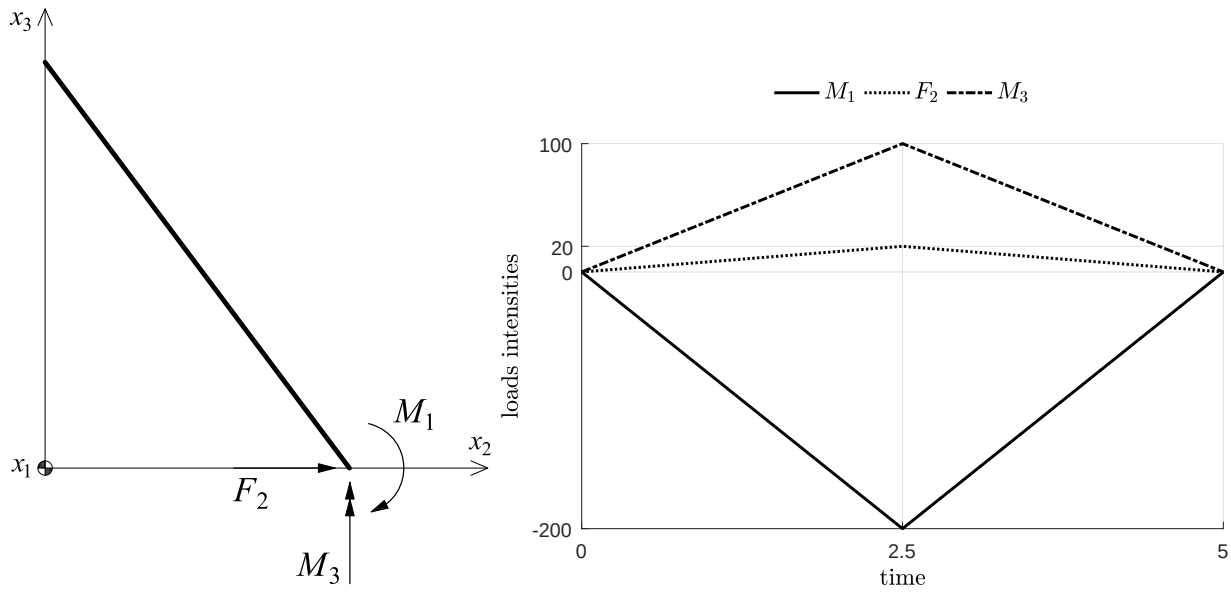

(a) Flying flexible beam subjected to force and moments.

(b) Load time histories for the flying flexible beam.

Figure 8: Flying flexible beam: initial configuration and loads.

Such a system of force and couples produces a complex deformation characterized by a forward translational motion due to F_2, a forward tumbling due to M_1 and an out-of-plane deformation due to M_3. In Figure 9, six snapshots of the flying flexible beam are shown projected on the (x_2, x_3) plane. Figure 10 shows five different snapshots projected on the (x_1, x_3) plane, and Figure 11 shows a three-dimensional view of ten snapshots. For each figure, the snapshots have been selected at the same time instants of [30] to facilitate the comparison. In order to assess the different role of time and space refinements, we present four cases: $p = 4$, $h = 1 \times 10^{-5}$ s; $p = 6$, $h = 1 \times 10^{-5}$ s, $p = 4$, $h = 5 \times 10^{-6}$ s and $p = 6$, $h = 5 \times 10^{-6}$ s, all with $n = 60$. All cases are in good qualitative agreement with results from the literature [30, 71]. Moreover, we note that the temporal error dominates the spatial one since no effects are seen after degree elevation. Indeed, given the same time step size, the solutions with $p = 4$ and $p = 6$ coincide. A similar effect is obtained by mesh refinement through knots insertion. Conversely, as visible in all figures, a slightly more accurate solution is obtained with $h = 5 \times 10^{-6}$ in comparison with $h = 1 \times 10^{-5}$, although both time step sizes lead to stable computations.

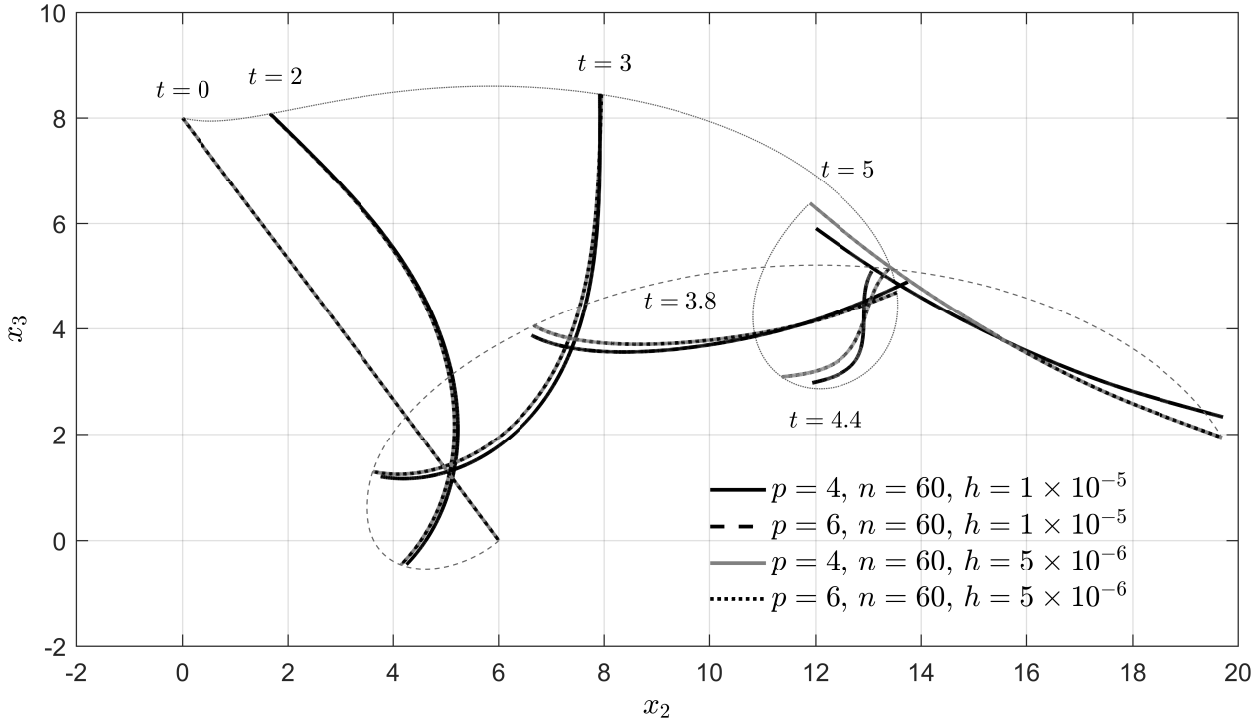

Figure 9: Snapshots of the free flexible flying beam in the early tumbling stage projected on the (x_2, x_3) plane.

6. Conclusions

Motivated by the goal of achieving higher-order accuracy in explicit dynamics through isogeometric collocation (IGA-C) methods, as recently demonstrated for linear elastodynamics, in this paper we explored the case of three-dimensional shear-deformable geometrically exact beams. Unlike in linear and traditional nonlinear structural dynamics, the configuration space of geometrically exact beams involves the rotation group SO(3) where standard time integration schemes cannot be directly used. Thus, the focus of the present work was on the development of a simple and SO(3)-consistent explicit time integration scheme. The work is intended as a first step towards the development of robust, efficient and higher-order accurate methods with potential applicability to all nonlinear structural elements (e.g. plates and shells) which share the same kinematic assumptions underpinning the present nonlinear beam model. We chose a kinematic model which completely avoids the use of linear transformation commonly employed to project incremental rotations belonging to different tangent spaces to SO(3), leads to a naturally singularity-free formulation due to the small

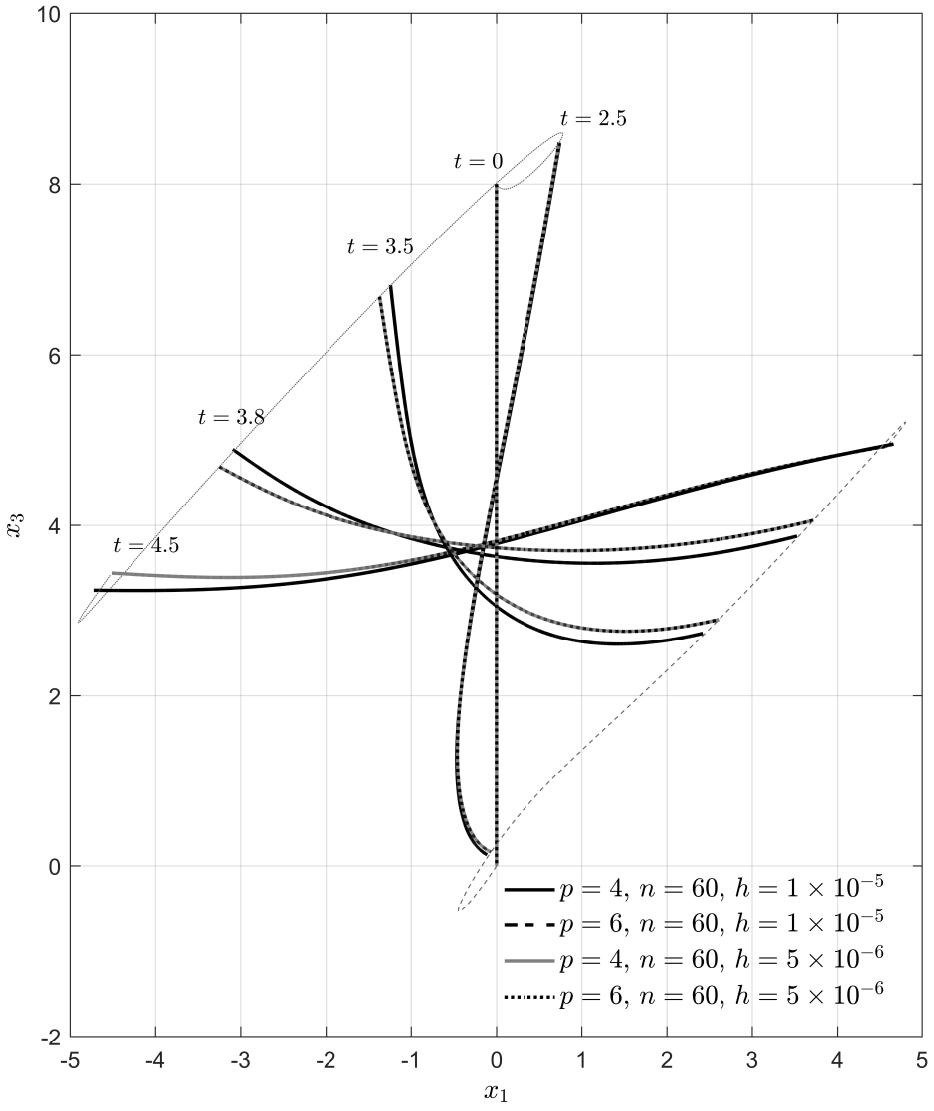

Figure 10: Snapshots of the free flexible flying beam in the early tumbling stage projected on the (x_1, x_3) plane.

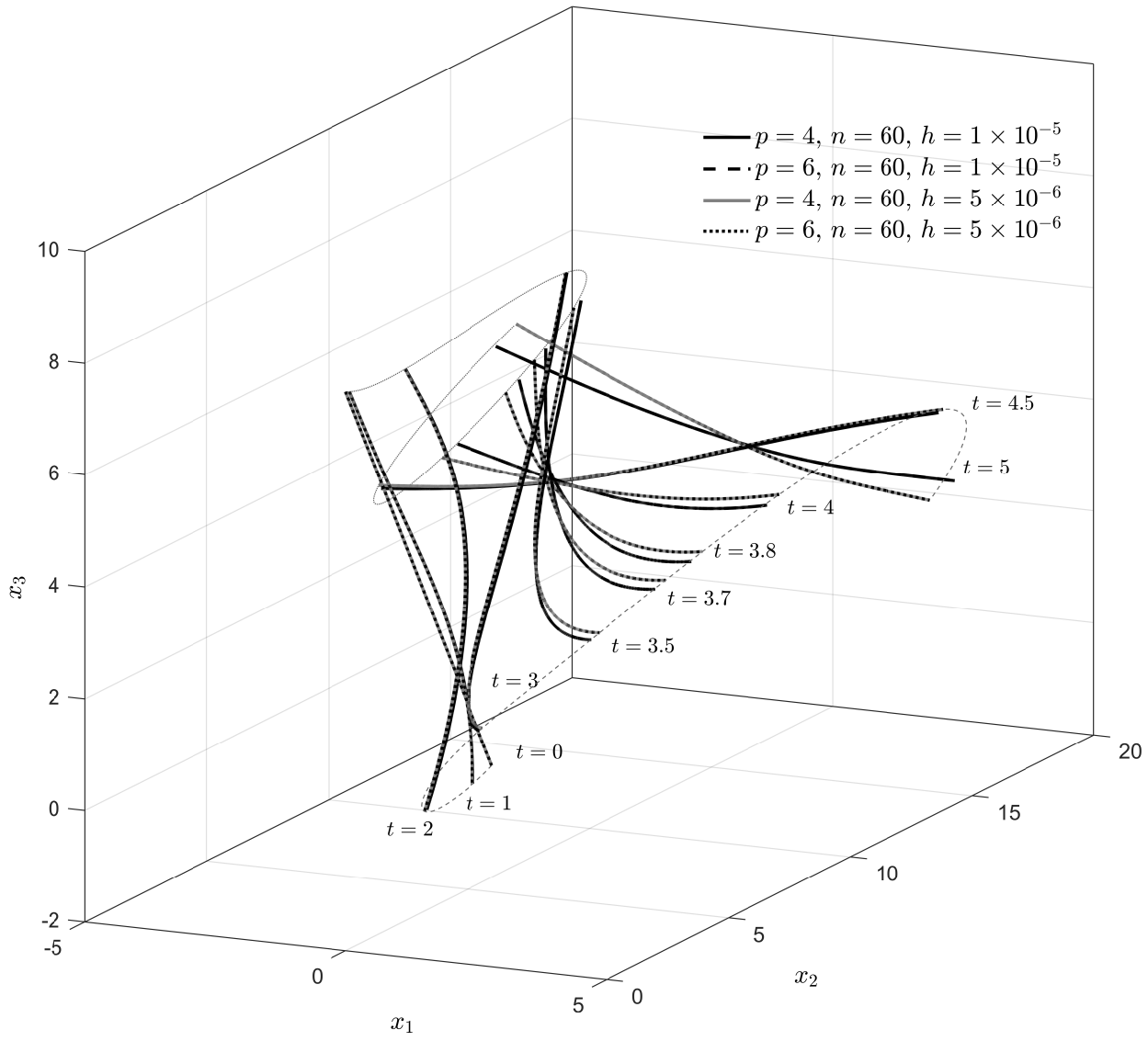

Figure 11: Snapshots of the free flexible flying beam in the early tumbling stage in a three-dimensional view.

sizes of the time steps, and does not require the collocation of additional equations, as for e.g. quaternion-based models, to guarantee the geometric consistency. We combined this kinematic model with one of the best-performing second-order accurate explicit Newmark time integrators for SO(3) originally proposed for rigid body dynamics. Update of the right-hand sides of the governing equations is performed straightforwardly within a geometrically consistent procedure once the primary control variables (angular and linear accelerations of the beam cross section) are computed from the previous time step. As opposed to the equations collocated in the interior points, where no linearization of the governing equations is needed, linearization is necessary for the Neumann boundary conditions.

The proposed formulation was applied to problems involving very large and fast rotations, considering different boundary conditions and stiffness properties of the beam. In all cases a very good agreement with literature results was obtained. Moreover, two observations, useful to provide guidance for future studies, were made: (i) the nonlinear term associated with the angular acceleration appearing in the time-discretized rotational balance equation has a negligible effect on the overall efficiency of the method since the Newton-Raphson algorithm converges always in one iteration regardless of size and velocity of the rotations; (ii) the overall accuracy is dominated by the temporal error. The first observation indicates that a linearized version of the rotational balance equation might be used instead of the original nonlinear one. We have already tested this possibility along with another critical simplification consisting in lumping mass and inertia matrices. Preliminary promising results not reported here were obtained, however, further work is still needed to guarantee the desired higher-order accuracy in space. The second observation indicates that developing SO(3)-consistent higher-order time-accurate schemes is of crucial importance in the development of explicit geometrically exact formulations.

Acknowledgements

Enzo Marino was partially supported by the DAAD scholarship program "Research Stays for University Academics and Scientists, 2018" (ref. no.: 91685958). This support is gratefully acknowledged. Josef Kiendl was supported by the Onsager fellowship program of NTNU. Laura De Lorenzis was supported by the DFG Priority Program SPP 1748 "Re-

liable Simulation Techniques in Solid Mechanics".

References

[1] F. Auricchio, L. B. Da Veiga, T. J. R. Hughes, a. Reali, G. Sangalli, Isogeometric Collocation Methods, Mathematical Models and Methods in Applied Sciences 20 (11) (2010) 2075–2107.

[2] F. Auricchio, L. Beirão da Veiga, T. J. R. Hughes, a. Reali, G. Sangalli, Isogeometric collocation for elastostatics and explicit dynamics, Computer Methods in Applied Mechanics and Engineering 249-252 (2012) 2–14.

[3] T. Hughes, J. Cottrell, Y. Bazilevs, Isogeometric analysis: CAD, finite elements, NURBS, exact geometry and mesh refinement, Computer Methods in Applied Mechanics and Engineering 194 (39-41) (2005) 4135–4195.

[4] Y. Bazilevs, L. Beirão da Veiga, J. Cottrell, T. J. R. Hughes, G. Sangalli, Isogeometric analysis: approximation, stability and error estimates for h-refined meshes, Mathematical Models and Methods in Applied Sciences 16 (07) (2006) 1031–1090.

[5] T. Hughes, A. Reali, G. Sangalli, Duality and unified analysis of discrete approximations in structural dynamics and wave propagation: Comparison of p-method finite elements with k-method NURBS, Computer Methods in Applied Mechanics and Engineering 197 (49-50) (2008) 4104–4124.

[6] J. A. Evans, Y. Bazilevs, I. Babuška, T. J. Hughes, n-Widths, supinfs, and optimality ratios for the k-version of the isogeometric finite element method, Computer Methods in Applied Mechanics and Engineering 198 (21-26) (2009) 1726–1741.

[7] L. da Veiga, A. Buffa, J. Rivas, G. Sangalli, Some estimates for $h-p-k-$refinement in isogeometric analysis., Numerische Mathematik 118 (2011) 271–305.

[8] C. Adam, T. Hughes, S. Bouabdallah, M. Zarroug, H. Maitournam, Selective and reduced numerical integrations for NURBS-based isogeometric analysis, Computer Methods in Applied Mechanics and Engineering 284 (2015) 732–761.

[9] F. Fahrendorf, L. De Lorenzis, H. Gomez, Reduced integration at superconvergent points in isogeometric analysis, Computer Methods in Applied Mechanics and Engineering 328 (2018) 390–410.

[10] G. Sangalli, M. Tani, Matrix-free weighted quadrature for a computationally efficient isogeometric k-method, Computer Methods in Applied Mechanics and Engineering 338 (2018) 117–133.

[11] D. Schillinger, J. Evans, A. Reali, M. Scott, T. J. Hughes, Isogeometric collocation: Cost comparison with Galerkin methods and extension to adaptive hierarchical NURBS discretizations, Computer Methods in Applied Mechanics and Engineering 267 (2013) 170–232.

[12] H. Gomez, A. Reali, G. Sangalli, Accurate, efficient, and (iso)geometrically flexible collocation methods for phase-field models., Journal for Computational Physics 262 (2014) 153–171.

[13] L. De Lorenzis, J. Evans, T. Hughes, A. Reali, Isogeometric collocation: Neumann boundary conditions and contact, Computer Methods in Applied Mechanics and Engineering 284 (2015) 21–54.

[14] R. Kruse, N. Nguyen-Thanh, L. De Lorenzis, T. Hughes, Isogeometric collocation for large deformation elasticity and frictional contact problems, Computer Methods in Applied Mechanics and Engineering 296 (2015) 73–112.

[15] H. Gomez, L. De Lorenzis, The variational collocation method, Computer Methods in Applied Mechanics and Engineering 309 (2016) 152–181.

[16] L. Beirão da Veiga, C. Lovadina, a. Reali, Avoiding shear locking for the Timoshenko beam problem via isogeometric collocation methods, Computer Methods in Applied Mechanics and Engineering 241-244 (2012) 38–51.

[17] F. Auricchio, L. Beirão da Veiga, J. Kiendl, C. Lovadina, a. Reali, Locking-free isogeometric collocation methods for spatial Timoshenko rods, Computer Methods in Applied Mechanics and Engineering 263 (2013) 113–126.

[18] J. Kiendl, F. Auricchio, T. Hughes, A. Reali, Single-variable formulations and isogeometric discretizations for shear deformable beams, Computer Methods in Applied Mechanics and Engineering 284 (2015) 988–1004.

[19] J. Kiendl, F. Auricchio, A. Reali, A displacement-free formulation for the Timoshenko beam problem and a corresponding isogeometric collocation approach, Meccanica (2017) 1–11.

[20] A. Reali, H. Gomez, An isogeometric collocation approach for Bernoulli-Euler beams and Kirchhoff plates, Computer Methods in Applied Mechanics and Engineering 284 (2015) 623–636.

[21] J. Kiendl, F. Auricchio, L. Beirão da Veiga, C. Lovadina, A. Reali, Isogeometric collocation methods for the Reissner-Mindlin plate problem, Computer Methods in Applied Mechanics and Engineering 284 (2015) 489–507.

[22] J. Kiendl, E. Marino, L. De Lorenzis, Isogeometric collocation for the Reissner-Mindlin shell problem, Computer Methods in Applied Mechanics and Engineering 325 (2017) 645–665.

[23] F. Maurin, F. Greco, L. Coox, D. Vandepitte, W. Desmet, Isogeometric collocation for Kirchhoff-Love plates and shells, Computer Methods in Applied Mechanics and Engineering 329 (2018) 396–420.

[24] E. Marino, Isogeometric collocation for three-dimensional geometrically exact shear-deformable beams, Computer Methods in Applied Mechanics and Engineering 307 (2016) 383–410.

[25] O. Weeger, S.-K. Yeung, M. L. Dunn, Isogeometric collocation methods for Cosserat rods and rod structures, Computer Methods in Applied Mechanics and Engineering 316 (2017) 100–122.

[26] O. Weeger, B. Narayanan, L. De Lorenzis, J. Kiendl, M. L. Dunn, An isogeometric collocation method for frictionless contact of Cosserat rods, Computer Methods in Applied Mechanics and Engineering 321 (2017) 361–382.

[27] E. Marino, Locking-free isogeometric collocation formulation for three-dimensional geometrically exact shear-deformable beams with arbitrary initial curvature, Computer Methods in Applied Mechanics and Engineering 324 (2017) 546–572.

[28] O. Weeger, B. Narayanan, M. L. Dunn, Isogeometric collocation for nonlinear dynamic analysis of Cosserat rods with frictional contact, Nonlinear Dynamics (2017) 1–15.

[29] J. A. Evans, R. R. Hiemstra, T. J. R. Hughes, A. Reali, Explicit higher-order accurate isogeometric collocation methods for structural dynamics, Computer Methods in Applied Mechanics and Engineering (2018) doi:10.1016/j.cma.2018.04.008.

[30] L. Simo, J. C. and Vu-Quoc, On the dynamics in space of rods undergoing large motions A geometrically exact approach, Computer Methods in Applied Mechanics and Engineering 66 (2) (1988) 125–161.

[31] A. Cardona, M. Geradin, A beam finite element non-linear theory with finite rotations, International Journal for Numerical Methods in Engineering 26 (September 1987) (1988) 2403–2438.

[32] A. Ibrahimbegović, M. A. L. Mikdad, Finite rotations in dynamics of beams and implicit time-stepping schemes 41 (November 1996) (1998) 781–814.

[33] G. Jelenic, M. a. Crisfield, Interpolation of Rotational Variables in Nonlinear Dynamics of 3D Beams, International Journal for Numerical Methods in Engineering 1222 (February 1997) (1998) 1193–1222.

[34] G. Jelenić, M. Crisfield, Geometrically exact 3D beam theory: implementation of a strain-invariant finite element for statics and dynamics, Computer Methods in Applied Mechanics and Engineering 171 (1-2) (1999) 141–171.

[35] J. Mäkinen, Critical study of Newmark-scheme on manifold of finite rotations, Computer Methods in Applied Mechanics and Engineering 191 (2001) 817–828.

[36] I. Romero, F. Armero, An objective finite element approximation of the kinematics of geometrically exact rods and its use in the formulation of an energy-momentum conserv-

ing scheme in dynamics, International Journal for Numerical Methods in Engineering 54 (12) (2002) 1683–1716.

[37] J. Mäkinen, Total Lagrangian Reissner's geometrically exact beam element without singularities, International Journal for Numerical Methods in Engineering 70 (October 2006) (2007) 1009–1048.

[38] J. Mäkinen, Rotation manifold SO(3) and its tangential vectors, Computational Mechanics 42 (6) (2008) 907–919.

[39] H. Lang, J. Linn, M. Arnold, Multi-body dynamics simulation of geometrically exact Cosserat rods, Multibody System Dynamics 25 (3) (2011) 285–312.

[40] O. Brüls, A. Cardona, M. Arnold, Lie group generalized-α time integration of constrained flexible multibody systems, Mechanism and Machine Theory 48 (2012) 121–137.

[41] E. Zupan, M. Saje, D. Zupan, Quaternion-based dynamics of geometrically nonlinear spatial beams using the RungeKutta method, Finite Elements in Analysis and Design 54 (2012) 48–60.

[42] E. Zupan, M. Saje, D. Zupan, Dynamics of spatial beams in quaternion description based on the Newmark integration scheme, Computational Mechanics 51 (1) (2013) 47–64.

[43] V. Sonneville, A. Cardona, O. Brüls, Geometrically exact beam finite element formulated on the special Euclidean group SE(3), Computer Methods in Applied Mechanics and Engineering 268 (3) (2014) 451–474.

[44] T.-N. Le, J.-M. Battini, M. Hjiaj, A consistent 3D corotational beam element for nonlinear dynamic analysis of flexible structures, Computer Methods in Applied Mechanics and Engineering 269 (2014) 538–565.

[45] P. M. Almonacid, Explicit symplectic momentum-conserving time-stepping scheme for the dynamics of geometrically exact rods, Finite Elements in Analysis and Design 96 (2015) 11–22.

[46] S. Eugster, Geometric Continuum Mechanics and Induced Beam Theories, Vol. 75, Springer, 2015.

[47] C. Meier, A. Popp, W. A. Wall, Geometrically Exact Finite Element Formulations for Slender Beams: Kirchhoff-Love Theory Versus Simo-Reissner Theory, Archives of Computational Methods in Engineering (2017) doi:10.1007/s11831-017-9232-5.

[48] L. Simo, J. C. and Vu-Quoc, A three-dimensional finite-strain rod model. Part II: Computational aspects, Computer Methods in Applied Mechanics and Engineering 58 (1) (1986) 79–116.

[49] A. Ibrahimbegovic, On the choice of finite rotation parameters, Computer methods in applied mechanics and engineerlng 149 (3) (1997) 49–71.

[50] M. Ritto-Correa, D. Camotim, On the differentiation of the Rodrigues formula and its significance for the vector-like parameterization of Reissner-Simo beam theory, International Journal for Numerical Methods in Engineering 55 (9) (2002) 1005–1032.

[51] S. Ghosh, D. Roy, A frame-invariant scheme for the geometrically exact beam using rotation vector parametrization, Computational Mechanics 44 (1) (2009) 103–118.

[52] P. Krysl, L. Endres, Explicit Newmark/Verlet algorithm for time integration of the rotational dynamics of rigid bodies, International Journal for Numerical Methods in Engineering 62 (15) (2005) 2154–2177.

[53] J. C. Simo, K. K. Wong, Unconditionally stable algorithms for rigid body dynamics that exactly preserve energy and momentum, International Journal for Numerical Methods in Engineering 31 (1) (1991) 19–52.

[54] G. Hulbert, Explicit momentum conserving algorithms for rigid body dynamics, Computers & Structures 44 (6) (1992) 1291–1303.

[55] Y. Choquet-Bruhat, C. Dewitt-Morette, Analysis, manifolds and physics Part I: Basics, Elsevier B.V., 1996.

[56] J. C. Simo, A finite strain beam formulation. The three-dimensional dynamic problem. Part I, Computer Methods in Applied Mechanics and Engineering 49 (1) (1985) 55–70.

[57] M. A. Crisfield, G. Jelenić;, Objectivity of strain measures in the geometrically exact three-dimensional beam theory and its finite-element implementation, Proceedings of the Royal Society of London A: Mathematical, Physical and Engineering Sciences 455 (1983) (1999) 1125–1147.

[58] R. K. Kapania, J. Li, On a geometrically exact curved/twisted beam theory under rigid cross-section assumption, Computational Mechanics 30 (5-6) (2003) 428–443.

[59] J. Argyris, An excursion into large rotations, Computer Methods in Applied Mechanics and Engineering 32 (13) (1982) 85–155.

[60] J. Stuelpnagel, On the Parametrization of the Three-Dimensional Rotation Group 6 (4) (1964) 422–430.

[61] H. Cheng, K. C. Gupta, An Historical Note on Finite Rotations, Journal of Applied Mechanics 56 (1) (1989) 139.

[62] J. E. Marsden, T. S. Ratiu, Introduction to Mechanics and Symmetry, 2nd Edition, Texts in Applied Mathematics, Springer, New York, NY, 1999.

[63] L. Piegl, W. Tiller, The NURBS Book, Springer, 1997.

[64] W. Rossmann, Lie groups An Introduction Through Linear Groups, oxford gra Edition, Oxford University Press, 2002.

[65] C. Anitescu, Y. Jia, Y. J. Zhang, T. Rabczuk, An isogeometric collocation method using superconvergent points, Computer Methods in Applied Mechanics and Engineering 284 (2015) 1073–1097.

[66] M. Montardini, G. Sangalli, L. Tamellini, Optimal-order isogeometric collocation at Galerkin superconvergent points, Computer Methods in Applied Mechanics and Engineering 316 (2017) 741–757.

[67] A. Gravouil, A. Combescure, Multi-time-step explicit-implicit method for non-linear structural dynamics, International Journal for Numerical Methods in Engineering 50 (1) (2001) 199–225.

[68] T. J. R. Hughes, The finite element method: linear static and dynamic finite element analysis, Dover Publications, 2000.

[69] S. Raknes, X. Deng, Y. Bazilevs, D. Benson, K. Mathisen, T. Kvamsdal, Isogeometric rotation-free bending-stabilized cables: Statics, dynamics, bending strips and coupling with shells, Computer Methods in Applied Mechanics and Engineering 263 (2013) 127–143.

[70] F. Maurin, L. Dedè, A. Spadoni, Isogeometric rotation-free analysis of planar extensible-elastica for static and dynamic applications, Nonlinear Dynamics 81 (1) (2015) 77–96.

[71] K. M. Hsiao, J. Y. Lin, W. Y. Lin, A consistent co-rotational finite element formulation for geometrically nonlinear dynamic analysis of 3-D beams, Computer Methods in Applied Mechanics and Engineering 169 (1-2) (1999) 1–18.

[72] R. Zhang, H. Zhong, A quadrature element formulation of an energymomentum conserving algorithm for dynamic analysis of geometrically exact beams, Computers & Structures 165 (2016) 96–106.